Characterization of ambient aerosol from measurements of cloud condensation nuclei during the 2003 Atmospheric Radiation Measurement Aerosol Intensive Observational Period at the Southern Great Plains site in Oklahoma

T. A. Rissman,[1] T. M. VanReken,[1] J. Wang,[2] R. Gasparini,[3] D. R. Collins,[3] H. H. Jonsson,[4] F. J. Brechtel,[1,5] R. C. Flagan,[1] and J. H. Seinfeld[1]

[1] Measurements were made by a new cloud condensation nuclei (CCN) instrument (CCNC3) during the Atmospheric Radiation Measurement (ARM) Program's Aerosol Intensive Observational Period (IOP) in May 2003 in Lamont, Oklahoma. An inverse aerosol/CCN closure study is undertaken, in which the predicted number concentration of particles available for activation (N_P) at the CCNC3 operating supersaturations is compared to that observed (N_O). N_P is based on Köhler Theory, with assumed and inferred aerosol composition and mixing state, and the airborne aerosol size distribution measured by the Caltech Dual Automatic Classified Aerosol Detector (DACAD). An initial comparison of N_O and N_P, assuming the ambient aerosol is pure ammonium sulfate (($NH_4)_2SO_4$), results in closure ratios (N_P/N_O) ranging from 1.18 to 3.68 over the duration of the IOP, indicating that the aerosol is less hygroscopic than ($NH_4)_2SO_4$. N_P and N_O are found to agree when the modeled aerosol population has characteristics of an external mixture of particles, in which insoluble material is preferentially distributed among particles with small diameters (<50 nm) and purely insoluble particles are present over a range of diameters. The classification of sampled air masses by closure ratio and aerosol size distribution is discussed in depth. Inverse aerosol/CCN closure analysis can be a valuable means of inferring aerosol composition and mixing state when direct measurements are not available, especially when surface measurements of aerosol composition and mixing state are not sufficient to predict CCN concentrations at altitude, as was the case under the stratified aerosol layer conditions encountered during the IOP.

1. Introduction

[2] One of the largest uncertainties in aerosol radiative forcing is associated with the indirect effect, which results from the relationship between atmospheric aerosols and cloud formation, properties, and lifetime [*Intergovernmental Panel on Climate Change*, 2001]. *Twomey* [1977] postulated that an increase in the number concentration of atmospheric aerosol particles would increase the number of cloud droplets formed for a given air mass. For fixed liquid water content, the cloud droplets would also be smaller than those formed under conditions with lower particle concentrations. This increase in number and decrease in mean diameter of cloud droplets would have two indirect effects on climate. Cloud albedo is greater for clouds with more numerous, smaller droplets; this has been termed the first indirect climatic effect of aerosols. Also, the lifetime of a cloud with smaller cloud droplets is greater than that of a cloud with larger droplets because the rain forming mechanisms are less efficient [*Albrecht*, 1989]. This is referred to as the second indirect climatic effect of aerosols. Both effects create clouds that are more reflective and more persistent, leading to the cooling of the Earth's surface [*Twomey*, 1977].

[3] The relationship between atmospheric particles that are capable of activating into cloud droplets, known as

[1]Department of Chemical Engineering, California Institute of Technology, Pasadena, California, USA.

[2]Brookhaven National Laboratory, Upton, New York, USA.

[3]Department of Atmospheric Sciences, Texas A&M University, College Station, Texas, USA.

[4]Center for Interdisciplinary Remotely Piloted Aircraft Studies, United States Naval Postgraduate School, Marina, California, USA.

[5]Brechtel Manufacturing, Inc., Hayward, California, USA.

cloud condensation nuclei (CCN), and aerosol size distribution and composition, in addition to meteorological conditions, are central to the indirect climatic effect of aerosols. For a given particle composition and size, the supersaturation above which the particle undergoes spontaneous condensational growth (activation) into a cloud droplet, the so-called critical supersaturation, is described by Köhler Theory. The activation diameter, the dry diameter at which a particle of known or assumed composition will activate, can also be calculated for a given supersaturation. Prediction of aerosol activation from Köhler Theory is very successful for aerosols composed of soluble, inorganic salts, such as ammonium sulfate ($(NH_4)_2SO_4$), sodium chloride (NaCl), and ammonium bisulfate (NH_4HSO_4). However, Köhler Theory needs to be augmented when considering chemical components, such as organic compounds, that are partially soluble, insoluble, or affect the surface tension of the aqueous solution. The chemical composition of atmospheric aerosol can be complex and include many different chemical species, which may affect aerosol activation in competing ways.

[4] The ability of Köhler Theory to predict ambient CCN concentrations can be studied by comparing atmospheric CCN measurements at a given supersaturation with CCN concentrations calculated using aerosol size distribution and composition measurements. This type of study, called an aerosol/CCN closure, compares the observed CCN concentration (N_O) at the operating supersaturation of the CCN instrument to that predicted from the aerosol size distribution and composition (N_P) in a closure ratio, defined here as N_P/N_O. N_P is determined from the aerosol size distribution by summing the concentration of particles with diameters greater than the activation diameter calculated from Köhler Theory [*VanReken et al.*, 2003]. When direct measurements of aerosol composition are unavailable, N_P can be calculated using an assumed aerosol composition or one that is inferred from other available measurements. An ''inverse'' aerosol/CCN closure study (explained further in section 5.2) can be undertaken to determine aerosol composition and mixing states that are most consistent with CCN observations when direct measurements of these aerosol characteristics are unavailable.

[5] In this paper, data measured by a new CCN instrument (CCNC3) during the Atmospheric Radiation Measurement (ARM) Aerosol Intensive Observational Period (IOP) in May 2003 are used in an inverse aerosol/CCN closure study of the midcontinental aerosol sampled near the Southern Great Plains (SGP) Central Facility (CF) to determine aerosol composition and mixing states consistent with the CCN measurements at the operating supersaturations of the instrument. The Texas A&M Differential Mobility Analyzer/Tandem Differential Mobility Analyzer (DMA/TDMA) data from the surface are used to infer the mixing state and insoluble fraction of the aerosol population as a function of dry diameter. This information is used with the airborne CCN and aerosol size distribution measurements to determine conditions under which aerosol composition and mixing states inferred from surface measurements are able to reproduce CCNC3 measurements at altitude. Aerosol properties, categorized by closure ratio and aerosol size

distribution shape, during pollution and smoke events are also discussed.

2. ARM Aerosol IOP

[6] The ARM Aerosol IOP occurred from 5 to 31 May 2003 at the Department of Energy's (DOE's) ARM SGP CF in Lamont, Oklahoma. There were a total of 16 science flights, with a total of 60.6 flight hours, conducted by the Center for Interdisciplinary Remotely-Piloted Aircraft Studies' (CIRPAS) Twin Otter aircraft on 15 days during this period. The ARM Aerosol IOP flight tracks for flights 6–10 and 12–17 (the flights for which there are CCN data) are shown in Figure 1, which illustrates that most flights took place over or near the SGP CF. The last flight, flight 17, was coordinated with the Moderate Resolution Imaging Spectroradiometer (MODIS) overpasses of four ARM sites (SGP CF, Extended Facility (EF)-12, EF-20, and EF-19 in Figure 1).

[7] The ARM SGP site is located in a midlatitude, continental area, surrounded by agricultural land and dirt roads. The site is influenced by local emissions from nearby industrial and power plants and local aerosol sources, such as vehicle and agricultural aerosols. Sulfur dioxide (SO_2) emissions from nearby oil refineries and power plants, such as the Conoco and Ponca City Power Plants, are major local sources of sulfate aerosols over the SGP site. Anthropogenic, agricultural related aerosol sources include local fertilizer application and production, field burning, and animal byproducts. Local biomass burning is greatest from May through July [*Iziomon and Lohmann*, 2003]. The particles that are commonly found at the ARM SGP site are a complex mix of these aerosol types, with smoke- and dust-dominated events, which are commonly characterized by decreased aerosol hygroscopicity, occurring occasionally [*Sheridan et al.*, 2001]. Routine condensation particle counter (CPC) measurements from the SGP site generally show a strong, diurnal cycle of aerosol number concentration, with peak concentrations in the afternoon and early evening. Over the 4-year period from July 1996 to June 2000, the daily average condensation nuclei (CN) concentration ranged from less than 1000 cm^{-3} to about 20,000 cm^{-3}, with a mean around 5000 cm^{-3}. The hourly average CN concentration ranged from about 4000 cm^{-3} from 1100 to 1500 UTC (Universal Time Coordinated) to about 18,000 cm^{-3} from 1800 to 2000 UTC [*Sheridan et al.*, 2001]. (The difference between local time (LT) at the ARM site and UTC is 5–6 hours, depending on daylight savings. During the ARM Aerosol IOP, LT was 5 hours behind UTC, so that 1200 LT corresponds to 1700 UTC in this paper.) These high CN concentrations could result from buildup and advection of pollutant aerosols from local sources, photochemical particle production [*Sheridan et al.*, 2001], coagulation, or the evolution of the boundary layer [*Iziomon and Lohmann*, 2003].

[8] Most of the Twin Otter flights during the ARM Aerosol IOP were conducted under clear or partly cloudy skies to assess aerosol impacts on solar radiation. Additional flights targeted mostly cloudy conditions to assess aerosol/cloud interactions, test theoretical understanding of aerosol activation, and to test surface remote sensing of the indirect effect. Ground and airborne measurements, which included
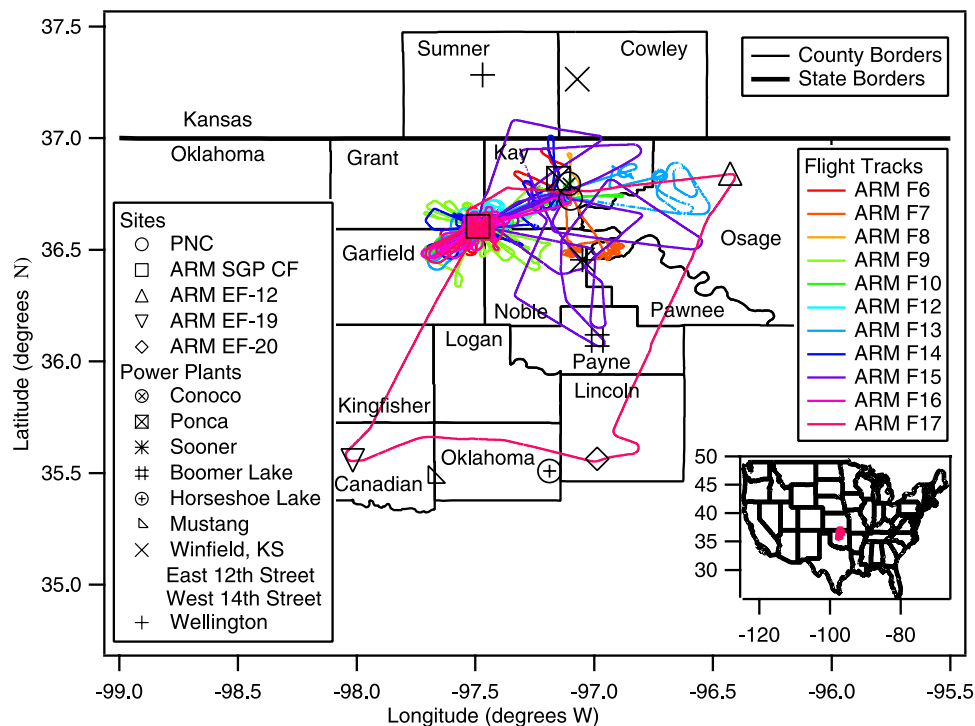
Figure 1. ARM Aerosol IOP flight paths for flights with CCN data. PNC is the Ponca City, Oklahoma, airport, where the Twin Otter was based. The other sites are ARM ground measurement sites. The insert shows the position of the counties (in pink) within the continental United States. The axes of the insert are in the same units as those in the main plot.

aerosol absorption, scattering, extinction, size distribution, and CCN concentration, are compared in a variety of closure studies to help resolve differences in measurements and models. Routine ARM SGP aerosol measurements (absorption, total scattering and hemispheric backscattering, light scattering as a function of relative humidity, total condensation particle concentration, number concentration of particles with diameters from 0.1 to 10 μm, vertical aerosol optical thickness, etc.) continued throughout the IOP.

## 3. Instrument Descriptions

3.1. Twin Otter Inlet System

[9] In order to minimize sampling losses, the aerosol inlet on the CIRPAS Twin Otter is designed to admit the air sample prior to any bending of flow lines and slow the sample down before transport to the instruments. The intake extends forward from the roof of the cabin to a position 1.2 m directly above the aircraft's nose. The sampled air is initially slowed down by a factor of 5 by means of an aerodynamically lipped diffuser. A second diffuser, positioned at the centerline of the first diffuser, reduces the flow speed by another factor of two, while excess flow from the first diffuser exits along the sides of the second diffuser. The sample then flows down a 7.62 cm diameter duct and enters the cabin after a 45° bend. Inside the cabin the duct is straightened out again with another 45° bend, and samples are drawn to the various instruments from ports mounted on the side of the duct. The ports are flush inside the duct, but extend outward at 45° angle to the flow. At an aircraft speed

of 50 m/s, approximately 1000 liters per minute (lpm) flow down the duct. Air not ciphered off to the instruments is dumped out of the cabin.

3.2. CCN Instrument (CCNC3)

[10] The CCN instrument (CCNC3) deployed on the Twin Otter consists of three columns, each of which is physically modeled after a previous CCN instrument column design [*Chuang et al.*, 2000] with some changes to the physical design. Three temperature-controlled sections are used to create the desired temperature gradient, instead of fourteen sections, as in the work by *Chuang et al.* [2000]. The instrument was designed to be fully automated and software controllable in normal operation and to operate with a different supersaturation in each column. CCNC3 operating conditions, some aspects of which differ from those given by *Chuang et al.* [2000], are discussed in the following paragraphs. Only column 1 operated properly during the ARM Aerosol IOP, the first field mission in which the CCNC3 was deployed; thus CCN data were obtained at one supersaturation per flight.

[11] Each CCNC3 column (Figure 2) consists of a stainless steel growth tube 0.4 m in length with a 1.9 cm outer diameter and a 1.6 mm wall thickness. The inner wall of the growth tube is lined with filter paper, which is rewetted by a small peristaltic pump every 90 min. Three temperature controlled, movable sections are in contact with the outer wall of the growth tube to create the desired temperature gradient, and, thus, the desired operating supersaturation, inside the growth tube. For the ARM Aerosol IOP, a linear temperature profile was used to develop a constant super-
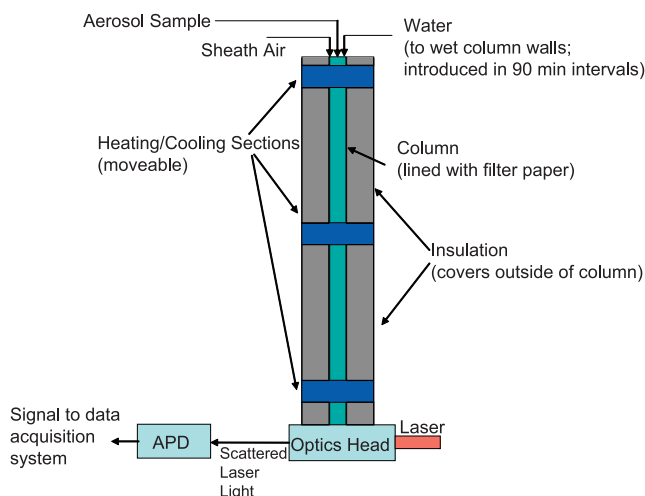
Figure 2. A schematic of a CCNC3 column. A second layer of insulation covers the growth tube and heating/cooling sections (to prevent temperature transfer to the outside air) and the detector (to prevent condensation within the optics tube).

saturation at the centerline of the growth tube [*Rogers and Squires*, 1977; *Roberts and Nenes*, 2005]. (A linear temperature gradient was also used in the airborne CCN instruments during the Cirrus Regional Study of Tropical Anvils and Cirrus Layers – Florida Area Cirrus Experiment (CRYSTAL-FACE) [*VanReken et al.*, 2003; *Roberts and Nenes*, 2005].) The sampled aerosol is focused onto the centerline of the growth tube and introduced to the column with filtered sheath air; the droplets that form within the growth tube are then counted by a detector.

[12] The CCNC3 detector consists of a laser, an optics tube, and an avalanche photo-diode (APD) module, and was designed on the basis of that of Laser Particle Counter (LPC) Model 3755 (TSI, Incorporated), scaled down for CCN application. A 670 nm, 10 mW Lasiris MFL Micro-Focus Laser is positioned at one end of an optics tube, so that the droplet inlet to the optics tube is at the 30 mm working distance of the laser. When a droplet falls through the laser beam, the laser light is scattered in the forward direction, and a pair of aspherical condenser lenses collects the scattered light and focuses it into a fiber optic at the other end of the optics tube. The signal from the scattered laser light is sent to a Hamamatsu Photonics C5460-01 APD module, which sends the resulting digital pulse to the data acquisition system.

[13] During the IOP, the column operated at three different linear temperature gradients, with one temperature gradient per flight. The total flow rate of the column was about 0.56 lpm with a sheath to sample ratio around 10. $(NH_4)_2SO_4$ calibrations for column 1 at its different linear temperature gradients are shown in Figure 3. The activation diameters and supersaturations associated with each linear temperature gradient are given in Figure 3. For each linear temperature gradient calibration, a solution of $(NH_4)_2SO_4$ was atomized to create droplets that were then dried and introduced into a differential mobility analyzer (DMA). Certain dry diameters were selected using the DMA and

then split to the CCNC3 inlet and the inlet to a CPC (TSI, Inc., Model 3010). The activated ratio (*AR*) was calculated as the ratio of the number concentration of CCN measured by the CCNC3 (N_{CCN}) to the number concentration of total particles measured by the CPC (N_{CPC}). The activation diameter (d_{act}) is the dry diameter at which 50% of the particles are activated ($AR = 0.5$). The uncertainty limits given on the calibration curves in Figure 3 result from the uncertainty in the diameter produced by the DMA (generally taken to be ±5%) and the combined uncertainties associated with the concentrations measured by the CPC and the CCNC3. These uncertainties associated with the column calibrations are folded into the overall measurement uncertainty, which is estimated for each flight on the basis of criteria explained in section 4.3.

[14] The supersaturation corresponding to dry $(NH_4)_2SO_4$ particles with diameter d_{act}, and thus the operating supersaturation of the column, was calculated theoretically by Köhler Theory. Droplet density is calculated from data of *Tang and Munkelwitz* [1994]; the full Pitzer model [*Pitzer*, 1973; *Pitzer and Mayorga*, 1973] is used to calculate the osmotic coefficient; and values from *Pruppacher and Klett* [1997] are used for surface tension. The model calculates the critical supersaturation for particles that contain certain soluble salts, certain organics, and generalized insoluble material [*Brechtel and Kreidenweis*, 2000a, 2000b].
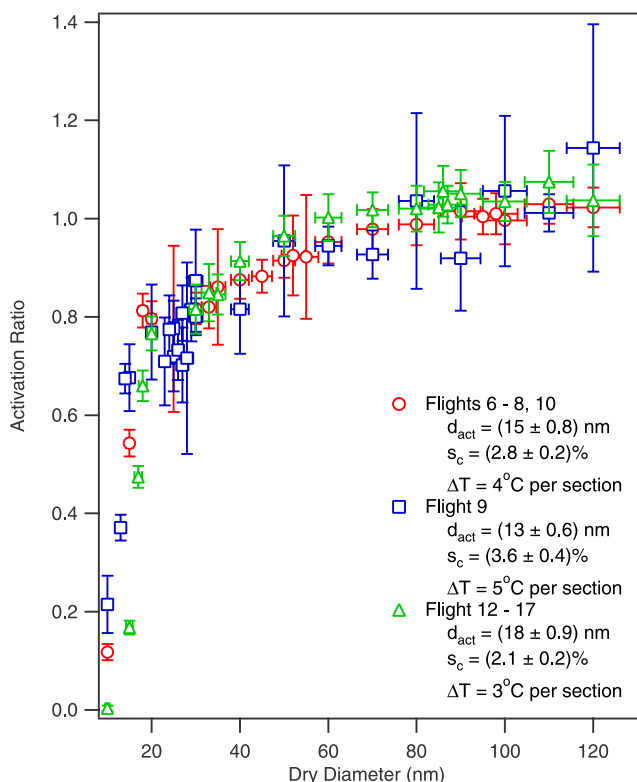
Figure 3. $(NH_4)_2SO_4$ calibration curves for column 1 of the CCNC3 at the temperature gradients used during the ARM Aerosol IOP. The column was not functioning properly for flights 1–5 and 11. The activation ratio is defined as the ratio of the number concentration of CCN measured by the CCNC3 to the number concentration of particles measured by the CPC.

Table 1. Flight Summary With Operating Conditions and Uncertainty Limits for CCNC3 Column 1

Flight	Day in May	Flight Begin Time,[a] UTC	Flight End Time,[a] UTC	Flight Length, Hours	Activation Diameter, nm	Operating Supersaturation, %	Upper Limit,[b] %	Lower Limit,[b] %
6	14	1553	2019	4.4	15 ± 0.8	2.8 ± 0.2	5	10
7	14	2124	2248	1.4	15 ± 0.8	2.8 ± 0.2	20	5
8	15	1634	1909	2.6	15 ± 0.8	2.8 ± 0.2	10	40
9	17	1402	1805	4.0	13 ± 0.6	3.6 ± 0.4	10	N/A
10	18	1543	1745	2.0	15 ± 0.8	2.8 ± 0.2	10	N/A
12	21	1551	1847	2.9	18 ± 0.9	2.1 ± 0.2	20	20
13	22	1325	1813	4.8	18 ± 0.9	2.1 ± 0.2	10	20
14	25	1852	2212	3.3	18 ± 0.9	2.1 ± 0.2	10	10
15	27	1420	1929	5.2	18 ± 0.9	2.1 ± 0.2	30	10
16	28	1824	2205	3.7	18 ± 0.9	2.1 ± 0.2	20	10
17	29	1411	1751	3.7	18 ± 0.9	2.1 ± 0.2	20	10

[a]The difference between local time (LT) and UTC was 5 hours during the ARM Aerosol IOP, so that 1200 LT corresponds to 1700 UTC.
[b]Uncertainty limits are reported as a percent of the measured concentration.

[15] The calibrated activation diameters and the operating supersaturations for column 1 during the ARM Aerosol IOP are given in the legend in Figure 3 and in Table 1. The instrument did not operate as expected from available instrument models and previous CCN instrument experience. Thermal contact between the temperature control sections and the growth column was improved in the design of the CCNC3. Therefore the CCNC3 requires a smaller temperature gradient than that required in previous CCN instruments to develop a similar supersaturation within the growth column. In-field calibrations were not available because the calibration CPC had been flooded with water. Therefore the operating supersaturations of the CCNC3 during the ARM Aerosol IOP were higher than would usually be desired for ambient aerosol studies. The consequences of these high supersaturations are further discussed in the Conclusion (section 7).

3.3. Dual Automatic Classified Aerosol Detectors (DACAD)

[16] The Caltech Dual Automatic Classified Aerosol Detectors (DACAD) have been deployed in several previous airborne experiments, and their characteristics are well documented [*Wang et al.*, 2002, 2003; *VanReken et al.*, 2003]. The DACAD consists of two DMA systems operated in parallel. One of the DMA systems measures the dry aerosol size distribution, while the other measures the aerosol size distribution at ambient relative humidity (RH) by using an active RH controller [*Wang et al.*, 2003]. The aerosol wet and dry size distributions are obtained separately and independent of each other; therefore no size-resolved information is obtained. The main components of the measurement system are a cylindrical DMA (TSI Inc., Model 3081) and a CPC (TSI Inc., Model 3010), which has a 50% counting efficiency at 10 nm. Using the scanning mobility technique, each DMA system generates a size distribution for particle diameters from ~17 to ~720 nm every 72.5 s [*Wang et al.*, 2002]. (This scanning time was reduced from 103 s [*VanReken et al.*, 2003] prior to the ARM Aerosol IOP.)

3.4. Tandem Differential Mobility Analyzer (DMA/TDMA)

[17] The Texas A&M DMA/TDMA measured aerosol size distributions and size-resolved hygroscopic growth at the SGP Cloud and Radiation Testbed (CART) trailer at the CF during the IOP [*Gasparini et al.*, 2006]. The main measurement section of the DMA/TDMA consists of two Aerosol Dynamics, Inc., high-flow DMAs (HF-DMAs [*Stolzenburg et al.*, 1998]), a charger, two Nafion tubes, and a CPC. One DMA/TDMA measurement sequence (~1 hour) consists of two different operational modes to obtain both the aerosol size distribution and the size-resolved hygroscopic growth. For both modes, the sample air is first dried in a Nafion tube and then introduced to a charger before entering the first DMA. During the single DMA mode (~5 min), the aerosol size distribution is measured by scanning the voltage applied to the first DMA [*Wang and Flagan*, 1990] and counting the size-selected aerosol particle concentration with the CPC. In TDMA mode, the voltage supplied to the first DMA is fixed to produce a monodisperse aerosol of known particle size. The monodisperse aerosol is exposed to a controlled, elevated relative humidity (RH; 85% in this IOP) before entering the second DMA. The humidified aerosol is classified by scanning the voltage applied to the second DMA and the size- and hygroscopicity-resolved aerosol particle concentration is observed with the CPC. The second mode sequence is repeated for other particle dry diameters by changing the voltage applied to the first DMA [*Gasparini et al.*, 2004]. A third mode was implemented during the IOP, in which the dry monodisperse aerosol was exposed to a wide range of RH to determine the deliquescence properties of the aerosol [*Gasparini et al.*, 2006].

[18] The aerosol particle soluble fraction and mixing state is inferred by comparing the dry diameter separated by the first DMA with the hydrated size distribution measured with the second DMA. The comparison results in a normalized distribution expressed in terms of the hygroscopic growth factor ($G(RH)$), which is defined as the ratio of the hydrated particle diameter to that of the dry particle. The aerosol is then divided into four hygroscopicity-based categories: pure insoluble, pure soluble, mixed insoluble, and mixed soluble. The full technique used to determine the relative contribution of soluble and insoluble components to the dry particle composition is described by *Gasparini et al.* [2004].

3.5. PILS-IC, TEOM, and Integrating Nephelometer

[19] At the SGP site, the aerosol ionic composition (species: NH_4^+, SO_4^{2-}, NO_3^-, K^+, Ca_2^+, Mg_2^+, Na^+, and Cl^-)

was measured using the Particle-Into-Liquid Sampler–Ion Chromatography (PILS-IC) technique [*Weber et al.*, 2001], and the aerosol total mass concentration was measured using the Tapered Element Oscillating Microbalance (TEOM) technique [*Patashnick and Rupprecht*, 1986]. The PILS-IC technique has a $\sim$0.05 μg m^{-3} limit of detection for all of the ions. The TEOM exhibited a temperature-related oscillation behavior during the IOP that resulted in an uncertainty of ±40%. The time resolution of the PILS-IC and TEOM were 8 min and 30 min, respectively, during the IOP. A sharp cut cyclone and two glass honeycomb denuders in series remove particles greater than 1 μm diameter and water-soluble vapor phase species, respectively, from the sample flow to both the PILS-IC and the TEOM. To prevent condensation of water within the tapered element, the TEOM inlet was maintained at 35°C [*Pahlow et al.*, 2006].

[20] Routine aerosol light scattering coefficient (σ_{sp}) and light scattering hygroscopic growth factor ($f(RH)$) measurements for total and fine (submicron) mode aerosol continued at the ground site during the IOP. Measurements of σ_{sp} and $f(RH)$ complement those from the PILS-IC and TEOM. Total scattering and backscattering were measured with a three-wavelength integrating nephelometer (TSI Inc., Model 3563) [*Sheridan et al.*, 2001]. The light scattering hygroscopic growth factor, $f(RH)$, is different from the hygroscopic growth factor ($G(RH)$) determined from DMA/TDMA data. $G(RH)$ is based on the increase in particle diameter with increasing RH (see section 3.4), whereas $f(RH)$ is defined as the change in aerosol light scattering with changing RH [*Covert et al.*, 1972; *Rood et al.*, 1987] and is determined as the ratio of σ_{sp} at 80% to that at 40% RH. $f(RH)$ was measured using a humidograph [*Carrico et al.*, 1998], which consists of two nephelometers separated by a humidity control system that ramps up the RH in the second nephelometer. Data from the humidograph are used to relate σ_{sp} at any RH to that at 40% RH with a three-parameter curve-fitting model [*Sheridan et al.*, 2001].

4. Data Trends During the ARM Aerosol IOP

4.1. Particle Composition (PILS-IC, TEOM, and DMA/TDMA) and Aerosol Mixing State (DMA/TDMA)

[21] Of the major inorganic ionic species (NH_4^+, SO_4^{2-}, NO_3^-, K^+, Ca_2^+, Mg_2^+, Na^+, Cl^-) measured at the SGP site during the IOP, NH_4^+ and SO_4^{2-} were dominant. NO_3^- was observed in $\sim$10% of the samples and only when SO_4^{2-} was completely neutralized by NH_4^+. K^+, a tracer for biomass burning, and Ca_2^+, a tracer for dust, were occasionally observed in appreciable levels. On average, the ratio of NH_4^+ to SO_4^{2-} was 2, with ratios significantly greater than 2 observed on 20 May (no flight) and 22 May (flight 13) and less than 2 observed on 21 May (flight 12) [*Pahlow et al.*, 2006].

[22] Aerosol organic fraction increased continuously during the daytime hours, while the inorganic concentration remained fairly constant. Overall, the aerosol organic content, which is estimated as the difference between total mass (TEOM) and total inorganic mass (PILS-IC), accounted for >40% of the aerosol mass. Increases in organic fraction, values of which were as high as 80%, were accompanied by a lowering of $f(RH)$, suggesting that the particulate organic fraction had a lower hygroscopicity than the inorganic fraction. Also, the amount of aerosol organic mass correlated strongly with the amount of black carbon inferred from the aerosol absorption coefficient [*Pahlow et al.*, 2006], which was measured using a filter-based light absorption photometer [*Sheridan et al.*, 2001].

[23] *Gasparini et al.* [2006] inferred size-resolved aerosol particle composition and hygroscopic growth properties from data collected by the Texas A&M DMA/TDMA at the SGP site using the technique from *Gasparini et al.* [2004]. The $G(RH)$ of the observed aerosol during the IOP was found to increase with increasing dry diameter, and the average median $G(RH)$ at 85% RH was 1.20 at 12 nm and 1.37 at 300 nm, which indicates that the smallest analyzed particles were largely composed of carbonaceous compounds. The largest particles were either very hygroscopic or slightly hygroscopic, but rarely exhibited hygroscopicity in between these extremes. At times during the IOP, a nonhygroscopic mode with median $G(RH)$ less than 1.10 was observed at 450 and 600 nm and, more rarely, at 200 and 300 nm [*Gasparini et al.*, 2006].

4.2. Aerosol Size Distribution (DACAD-Airborne)

[24] The aerosol size distributions measured by the DACAD were analyzed for flights 6–10 and 12–17, for which CCN data were collected. Aerosol size distributions differed greatly between flights, as well as at different altitudes within a single flight. For example, Figure 4 shows DACAD aerosol size distributions from six level legs and five different altitudes from flight 16. At the lower altitudes, 351 m and 720 m AGL (Above Ground Level; all reported altitudes are AGL), the aerosol size distributions are multimodal with median diameters less than the cutoff diameter of the DACAD ($\sim$17 nm), which may indicate that the sampled aerosols are freshly emitted or formed locally in the atmosphere. The aerosol populations at 1028 m and 1337 m have similar size distributions that are multimodal with median diameters that may be smaller than the cutoff diameter of the DACAD, which may indicate mixed aerosol layers that are a combination between fresh and aged aerosol populations. The aerosol population at 2281 m during flight 16 is multimodal but with a less pronounced second mode at larger diameters, which is indicative of background aerosol. Also note that the $dN/dlogD_p$ values are greater for lower-altitude level legs than higher legs, which is a typical feature of ambient aerosol. Aerosol size distributions such as those shown in Figure 4 were seen throughout the IOP flights, along with some simple unimodal distributions. The differences in aerosol size distributions are consistent with sampled aerosol layers that had different sources and/or were of different ages.

[25] Rapidly changing aerosol size distributions were observed frequently during the IOP. Since the DACAD size distribution scan time is 72.5 s, some characteristics of a rapidly changing aerosol size distribution may not have been resolved. The CCNC3 has a sampling rate of 1 s and, therefore, is capable of observing rapid changes in the aerosol size distribution. For this reason, predicted and observed CCN concentrations may not agree well during
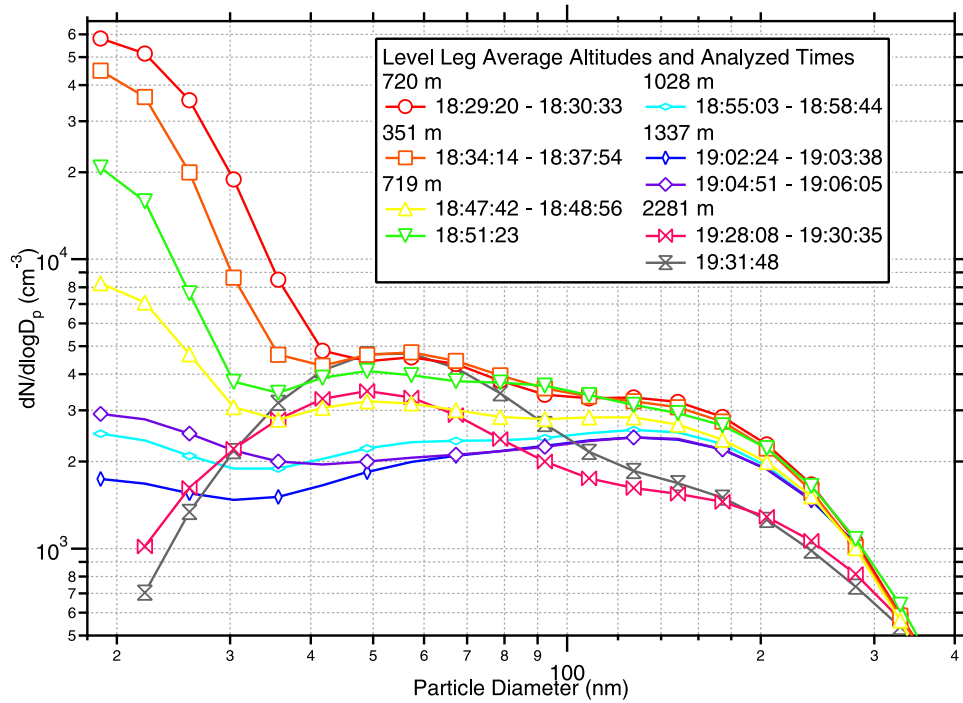
Figure 4. Aerosol size distributions from different level legs during flight 16. The legend gives the average altitudes (AGL) and times analyzed for each level leg. The times given are UTC; 1700 UTC corresponds to 1200 LT.

times of rapidly changing aerosol characteristics. This will be discussed further in section 6.

4.3. CCN Concentration (CCNC3-Airborne)

[26] The trends in the CCN concentration data follow those seen in both the airborne CPC and airborne DACAD data. When present, homogeneous boundary layers are easily discerned from plots of CCNC3, CPC, and DACAD data, e.g., Figure 5 for flight 14. A more specific CCN trend analysis is discussed in section 6.

[27] The airborne CPC had a cutoff diameter of 13 nm, and the DACAD scanned particle sizes down to ~17 nm.
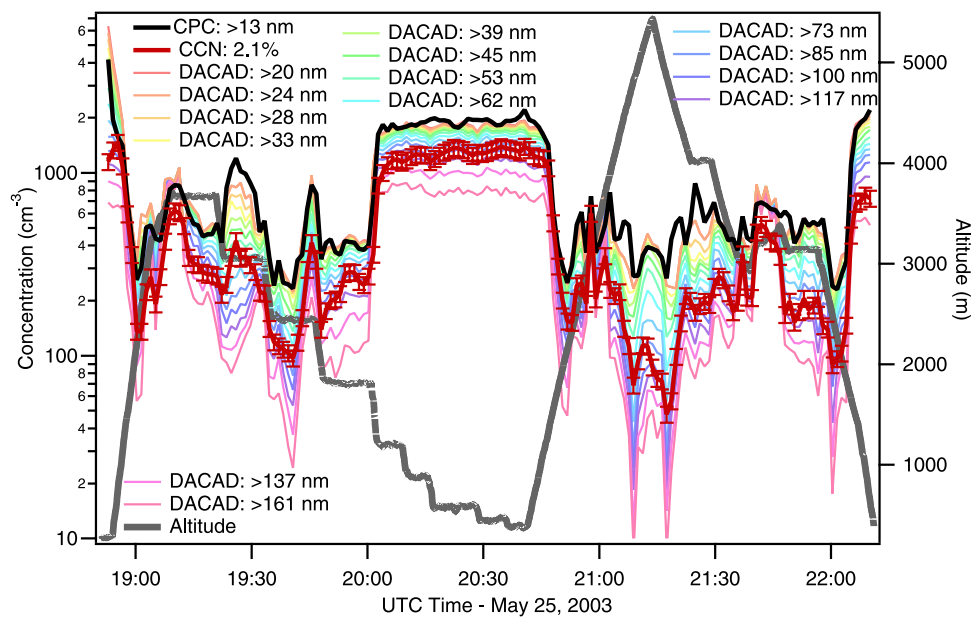
Figure 5. Flight traces of CPC, CCNC3, and DACAD data for flight 14. The DACAD traces give the total concentrations of particles with diameters greater than those noted in the legend. A well-mixed boundary layer is clearly shown from about 2010 to 2045. The times given are UTC; 1700 UTC corresponds to 1200 LT.
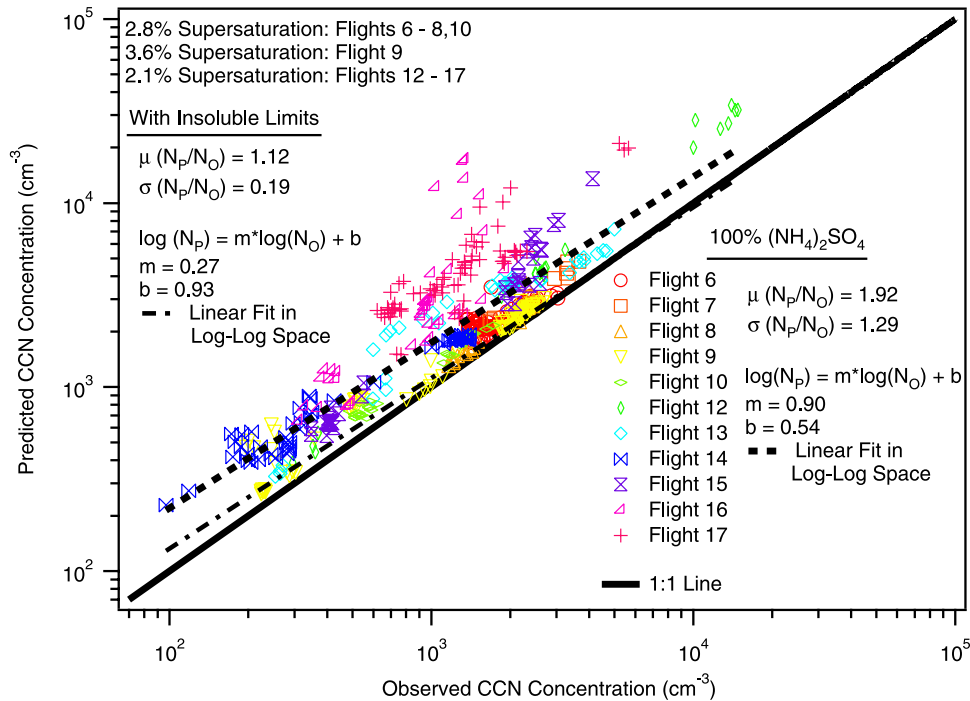
Figure 6. Predicted CCN concentration (N_P; assuming pure $(NH_4)_2SO_4$) versus observed CCN concentration (N_O) for ARM Aerosol IOP. Only flights for which CCN data are available are shown. N_P is determined from the DACAD size distribution for all flights except flight 9, for which N_P is determined from the CPC total particle (>13 nm) concentration. The linear fit in log-log space for all flight closure data is shown, and corresponding fit parameters are given. The mean and standard deviation of the ratio of N_P to N_O averaged over all flights are also given. The fit parameters and mean and standard deviation of the ratio of N_P to N_O are also shown for the "Insoluble Limit" case, for which N_P is calculated using the insoluble fractions calculated in section 5.2.1.

The CCN number concentrations are always less than the total particle number concentrations measured by the CPC or the DACAD in any of the eleven flights, even though the activation diameters for pure $(NH_4)_2SO_4$ particles at the operating supersaturations of the CCNC3 are similar to the cutoff diameters for the CPC and DACAD. To determine the uncertainty in the CCN measurements, the CPC concentration was used as a high-end limit for CCN concentration on all flights. The concentration measured by the CCNC3 column 2, when operating, was used as the lower limit for the column 1 CCN concentration. The operating supersaturation of column 2 was unable to be determined with any certainty, but it was always operating at some supersaturation lower than that of column 1. Therefore measurements by column 2 are used as estimates of the lower uncertainty limit for the measurements of column 1, when both columns were operating, but are not used in any other part of the analysis. Table 1 gives the uncertainty limits for column 1.

5. Inverse Aerosol/CCN Closure Study: Results and Discussion

[28] Comparison of the CCN data to the aerosol size distribution data allows certain conclusions to be drawn about the characteristics of the measured CCN and the aerosol population. Certain aerosol population properties,

such as particle insoluble fraction or mixing state, can be estimated as those that lead to closer agreement between predicted and observed CCN concentrations at the operating supersaturations of the CCN instrument. These estimated properties can be compared with those inferred from or measured by other instruments to determine whether the estimates are reasonable.

[29] For this study, the CCN data sets were averaged over the scan time of the DACAD (72.5 s) to correspond with a single aerosol size distribution. Scans during which the standard deviation of the CCN data exceeded 15% of the mean of the CCN data were removed from the inverse closure analysis. This helps to remove intervals during which the aerosol size distribution may be changing sufficiently rapidly during the 72.5 s scan time of the DACAD that the changes are not resolved in aerosol size distribution measurements. One further constraint: only data measured during level legs of flight patterns were included to ensure that the CCNC3 inlet pressure was steady and did not cause any rapid changes or instability in the CCN sample flow rate, although this artifact was not observed even during rapid ascents and descents. Data measured within clouds were also removed from the inverse aerosol/CCN closure analysis to exclude the potential influence of artifact particles resulting from cloud droplet shattering in the Twin Otter inlet. The DACAD did not operate at altitudes above about ~3000 m (except during flight 14), so the inverse

Table 2. Average ($\mu(N_P/N_O)$) and Standard Deviation ($\sigma(N_P/N_O)$) of the Ratios of Predicted CCN Concentration to Observed CCN Concentration for All Flights for Which There Were CCN Data[a]

Flight	Day in May	$\mu(N_P/N_O)$	$\sigma(N_P/N_O)$	m	b	R^2	Number of Data Points
6	14	1.30	0.18	0.63	1.32	0.63	80
7	14	1.29	0.13	0.81	0.77	0.96	11
8	15	1.18	0.07	1.05	−0.10	0.96	55
9	17	1.29	0.35	0.85	0.54	0.96	78
10	18	1.34	0.08	0.97	0.21	0.98	27
12	21	1.79	0.36	1.14	−0.22	0.99	23
13	22	1.78	0.51	0.91	0.51	0.90	38
14	25	1.84	0.48	0.77	0.88	0.96	54
15	27	1.87	0.45	1.14	−0.18	0.97	38
16	28	3.68	2.96	1.40	−0.68	0.65	42
17	29	3.45	0.86	0.93	0.74	0.77	71
All		1.92	1.29	0.90	0.54	0.74	517

[a]Slope (m) and intercept (b) values for linear fits of N_P to N_O in log-log space are also given. Assumes pure $(NH_4)_2SO_4$ in the calculation of N_P.

aerosol/CCN closure analysis generally does not include data above this altitude.

5.1. Inverse Aerosol/CCN Closure: Initial Comparison, Assuming 100% $(NH_4)_2SO_4$

[30] Figure 6 shows an initial comparison of the predicted CCN number concentrations (N_P) to those observed by the CCNC3 instrument (N_O) for all eleven flights and includes all the data points from each flight that fit the criteria outlined in section 5. For this initial comparison, N_P is determined as the sum of the number concentration of particles in the DACAD size distributions with diameters greater than the activation diameter of an aerosol consisting of pure $(NH_4)_2SO_4$ for the operating supersaturation of the CCN instrument. Pure $(NH_4)_2SO_4$ is assumed as a starting point because PILS-IC data from the ground indicated that NH_4^+ and SO_4^{2-} were dominant species and that the average ratio of NH_4^+ to SO_4^{2-} was near 2 during the ARM Aerosol IOP. For flight 9, N_P is determined from the CPC total particle concentration, since the activation diameter of the CCNC3 column is about the same as the cutoff diameter for the CPC. The average value of N_P/N_O ($\mu(N_P/N_O)$) for all flights is 1.92, with a standard deviation ($\sigma(N_P/N_O)$) of 1.29, and Table 2 shows this ratio for each flight. ($\mu(N_P/N_O)$ is used when values of the ratio, N_P/N_O, have been averaged over more than one DACAD scan.) The average value of N_P/N_O for each flight, and thus for all flights averaged together, is greater than unity. This indicates that fewer particles activated than would be expected if the particles were composed of pure $(NH_4)_2SO_4$. The average N_P/N_O also differs from flight to flight, which indicates that the aerosol CCN activity properties changed from flight to flight.

[31] The N_P versus N_O data for each flight were fit to a straight line in log-log space, and the results for the slope and intercept of those fits are given in Table 2. The fit for all data is shown in Figure 6, and Figure 7 shows the fit for flights 8, 12, 14, and 17. Nonunity slopes and nonzero intercepts of these linear fits in log-log space offer some insight as to the characteristics of the ambient aerosol population through its deviation from the activation properties of pure $(NH_4)_2SO_4$ particles.

[32] The slopes of the log-log fit of N_P versus N_O for the IOP flights are generally not unity, which indicates that the chemistry and mixing state of the aerosol population does not affect the CCN ability at all concen-

trations equally. This imbalance results from sampling different air masses with different aerosol properties, which lead to different N_P to N_O ratios, during the same flight. Aerosol populations with low CCN concentration, which often result from those with low total particle concentration (N_{Total}), tend to have "clean" aerosol sources or be well-aged aerosols, in which particle coagulation has decreased N_{Total} and cloud processing has likely increased soluble fractions. These types of air masses with low CCN concentrations would have N_P to N_O ratios nearer to unity. High N_{Total}, on the other hand, is often indicative of fresh, polluted aerosol sources, possibly with high levels of insoluble material and a greater degree of external mixing, which could lead to higher values (greater than unity) of N_P/N_O. In Figure 7, the clustering of flight 12's closure data points at low, medium, and high CCN concentrations could indicate that three different air masses were sampled. The air mass with midlevel CCN concentrations could be a mixture of the air masses with high- and low-level CCN concentrations, instead of a distinct air mass. Figure 8 illustrates trends of N_P/N_O with altitude as a function of longitude for flights 12 (Figure 8a) and 14 (Figure 8b). The high CCN concentration data points (Figure 7) for flight 12 correspond to the N_P/N_O points (Figure 8) at altitudes of about 600 m ($N_P/N_O = 2.77$), 850 m ($N_P/N_O = 1.99$–2.42), and 1380 m ($N_P/N_O = 2.00$); the mid CCN concentration data points correspond to the N_P to N_O ratios at about 550 m ($N_P/N_O = 1.51$–2.02), 600 m ($N_P/N_O = 1.77, 1.80$), and 1380 m ($N_P/N_O = 1.67$); and the low CCN concentration points correspond to the N_P to N_O ratios at about 2100 m ($N_P/N_O = 1.23$–1.53).

[33] The situation is quite different for flight 14 (see Figures 7 and 8), for which the generalized high and low N_{Total} classifications do not hold. All of the closure data points from flight 14 are clustered at CCN concentrations less than 2000 cm^{-3}, and the slope is less than unity. Contrary to what was observed in flight 12, the sampled aerosol with lower N_{Total} has a greater deviation from idealized, pure $(NH_4)_2SO_4$ particles than those with higher N_{Total}. As will be discussed later in section 6, flight 14 was apparently influenced by a Siberian smoke event [*Schmid et al.*, 2004]. Smoke aerosols that have been transported a long distance are likely to have low particle concentrations through particle coagulation and cloud processing. However, the aged smoke particles at low N_{Total} in flight 14 did not
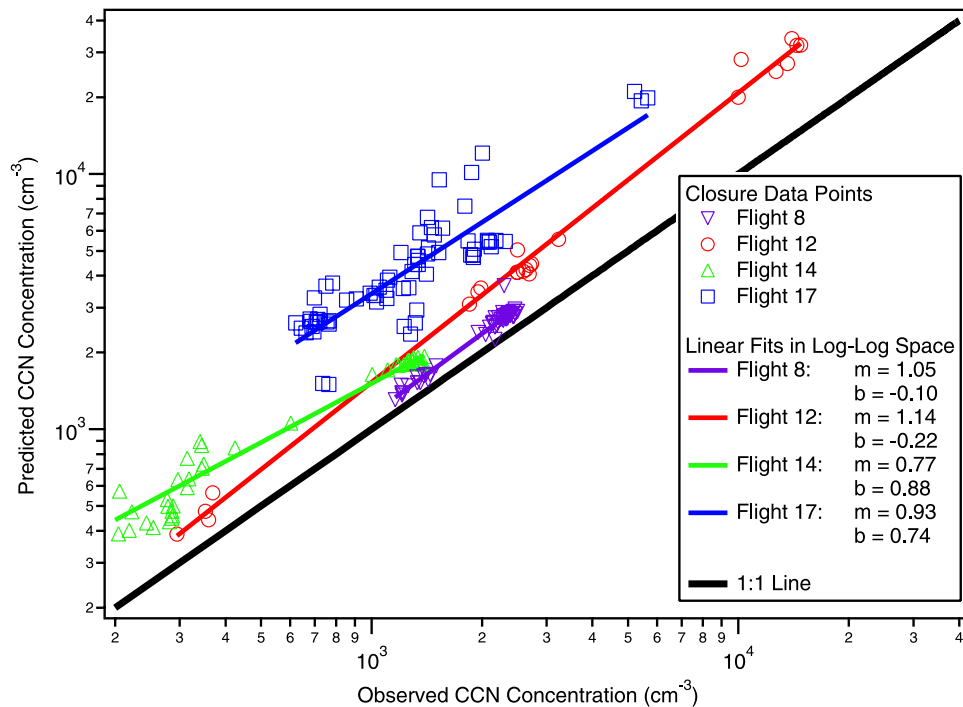
Figure 7. N_P (assuming pure $(NH_4)_2SO_4$) versus N_O and linear fits in log-log space for flights 8, 12, 14, and 17. High aerosol concentrations (from the CPC) were 10,400 cm^{-3}, 37,000 cm^{-3}, 3550 cm^{-3}, and 2890 cm^{-3} for flights 8, 12, 14, and 17, respectively. High CCN concentrations were 2882 cm^{-3}, 16,941 cm^{-3}, 2143 cm^{-3}, and 7454 cm^{-3} for flights 8, 12, 14, and 17, respectively. High concentration values were determined as the maximum concentrations measured after the Twin Otter had achieved sampling altitude after takeoff, regardless of whether the data were obtained during constant altitude legs.

become more CCN active than the background aerosol, which is probably the type of aerosol sampled under about 1400 m (see Figure 8).

[34] An intercept that deviates from zero indicates that some fraction of the aerosol population is unavailable for activation at the measurement supersaturation, although this fraction would activate under the assumption of pure $(NH_4)_2SO_4$ particles. This nonactive fraction could consist of particles from an internal or external mixture that have some fraction of insoluble, hydrophobic material that prevents activation. Even if the slope were near unity, the intercept can, as explained above, deviate from zero if particles exist that do not exhibit predicted CCN activity characteristics. Flights 8 and 17 (Figure 7) have slopes near unity but have very different intercepts, even though their observed CCN concentrations are within a similar range. HYSPLIT [*Draxler and Rolph*, 2003; *Rolph*, 2003] 3-day back trajectories for flights 8 and 17 (Figures 9 and 10, respectively) show that the sampled air masses from flights 8 and 17 originated in different areas, with those from flight 8 being more influenced by marine conditions in the Gulf of Mexico and those from flight 17 being more influenced by inland continental conditions. DACAD size distributions from the analyzed times during flight 8 are bimodal, with no indication of sampled pollution events, and $dN/dlogD_P$ values were less than 5000 cm^{-3}. Flight 17, however, was dominated by pollution events, as is indicated by its primarily multimodal size distributions that are dominated by particles with diameters smaller than 50 nm. Measured $dN/dlogD_P$ values for flight 17 were as high as 60,000 cm^{-3},

but most were under 10,000 cm^{-3}. It makes sense, then, that the deviation of flight 17's intercept from zero is greater than that of flight 8 because fewer particles are available for activation under polluted than clean conditions. When the slope is not near unity, the intercept can be affected by differences in CCN activities among the sampled air masses and may not have a simple interpretation.

[35] On the basis of this initial comparison of N_O and N_P determined from DACAD size distributions with the assumption of 100% $(NH_4)_2SO_4$, it is apparent that more detailed aerosol properties, such as chemical composition and the mixing state, are needed to predict the CCN measurements at the operating supersaturations of the CCNC3. Because such composition and mixing data were, however, unavailable on the Twin Otter during the IOP, an inverse closure study is performed, in which the comparison of N_O and N_P based on the assumption of pure $(NH_4)_2SO_4$ is used to infer the aerosol composition and mixing state that are consistent with CCN observations.

5.2. Inverse Aerosol/CCN Closure: Inferring Deviations From 100% $(NH_4)_2SO_4$

[36] An inverse aerosol/CCN closure evaluates the extent to which particle composition alone can explain the discrepancy between N_P and N_O. Particle composition can be modeled as an internal or an external mixture and can consist of completely soluble and insoluble material or include partially soluble material, as well. For the purposes of the study presented here, particle components are considered to be either completely soluble or completely
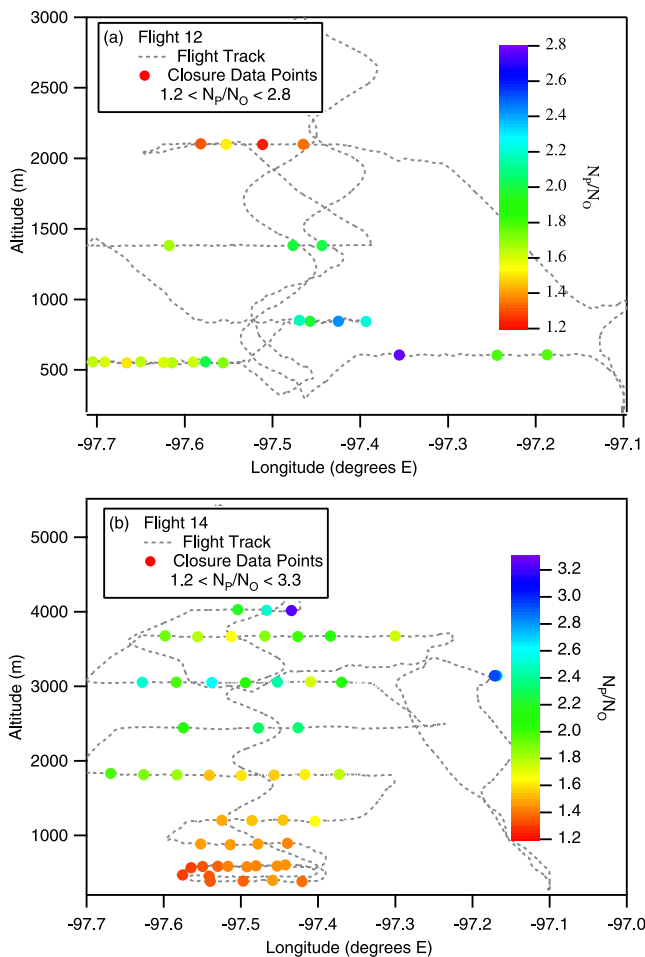
Figure 8. Altitude versus longitude trace for flights (a) 12 and (b) 14. Closure data points are indicated by the solid circles. The color of the closure data points indicates the magnitude of N_P/N_O, assuming pure $(NH_4)_2SO_4$, for the corresponding DACAD scan.

insoluble, and both internally and externally mixed aerosol populations are considered. Although the customary definition of an internal mixture is that all particles of the same size have the same chemical composition, a more simplified, size-independent internal mixture is used here in the absence of airborne measurements of size resolved chemistry. Thus, under the assumption of a size-independent internally mixed aerosol population, all particles of all diameters have the same fractional insoluble/soluble composition in this analysis. An external mixture can include purely soluble particles, purely insoluble particles, and particles composed of both insoluble and soluble material.

### 5.2.1. Estimating Aerosol Particle Composition From CCNC3 and DACAD Measurements

[37] The initial comparison of N_P and N_O (from section 5.1) can be used to determine the particle volumetric fraction of insoluble material (ε_{ins}) that would be necessary for $\mu(N_P/N_O)$ to approach unity, assuming that the ambient aerosol is a size-independent internal mixture, with particles of all sizes having insoluble fraction ε_{ins}. In order to calculate ε_{ins} for each flight, the cumulative aerosol size distribution is determined, with each size

bin containing the concentration of all particles with diameters greater than the bin diameter. For each analysis period, the DACAD midbin diameter for which the cumulative aerosol concentration approaches the measured CCN concentration is chosen as the cutoff diameter, defined as the dry diameter above which sampled ambient particles would be able to activate under the assumption of size-independent internal mixing. A value for ε_{ins} is determined by inputting the cutoff diameter and different values of ε_{ins} (with the balance $(NH_4)_2SO_4$) into the Köhler Theory model, until the particle's calculated critical supersaturation approaches the operating supersaturation of the CCNC3.

[38] Since the sampled air mass properties typically varied widely during a flight, this analysis is carried out for each level leg during each flight. A level leg is defined as one for which consecutive static pressure measurements are constant within ±3 mbar. Some level legs are further divided if it appears that drastically different air masses were sampled during the same level leg. This usually occurs for level legs that cover long distances but was observed even during some shorter-distance legs. Table 3 gives the range and mean of ε_{ins} values for each flight. Most of the values of ε_{ins} that are required for $\mu(N_P/N_O)$ to approach unity exceed 0.90, with only 14 out of the 113 analyzed level legs having ε_{ins} values less than 0.90. While insoluble mass fractions in aerosol particles in continental areas have been found as high as 0.98, values less than 0.6 are more
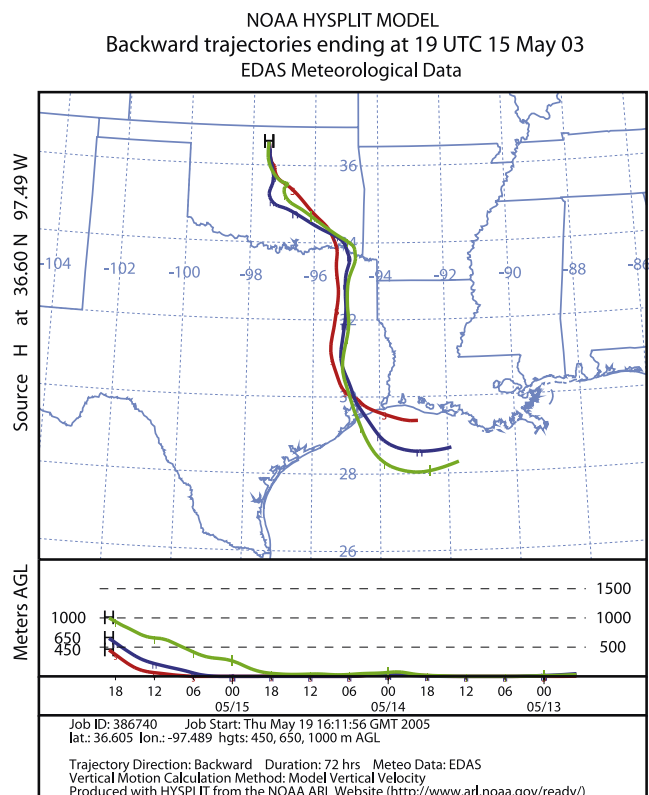
Figure 9. Three-day HYSPLIT back trajectories for 15 May 2003 (flight 8) at the SGP site at altitudes of 450, 650, and 1000 m. The times given are UTC; 1700 UTC corresponds to 1200 LT.
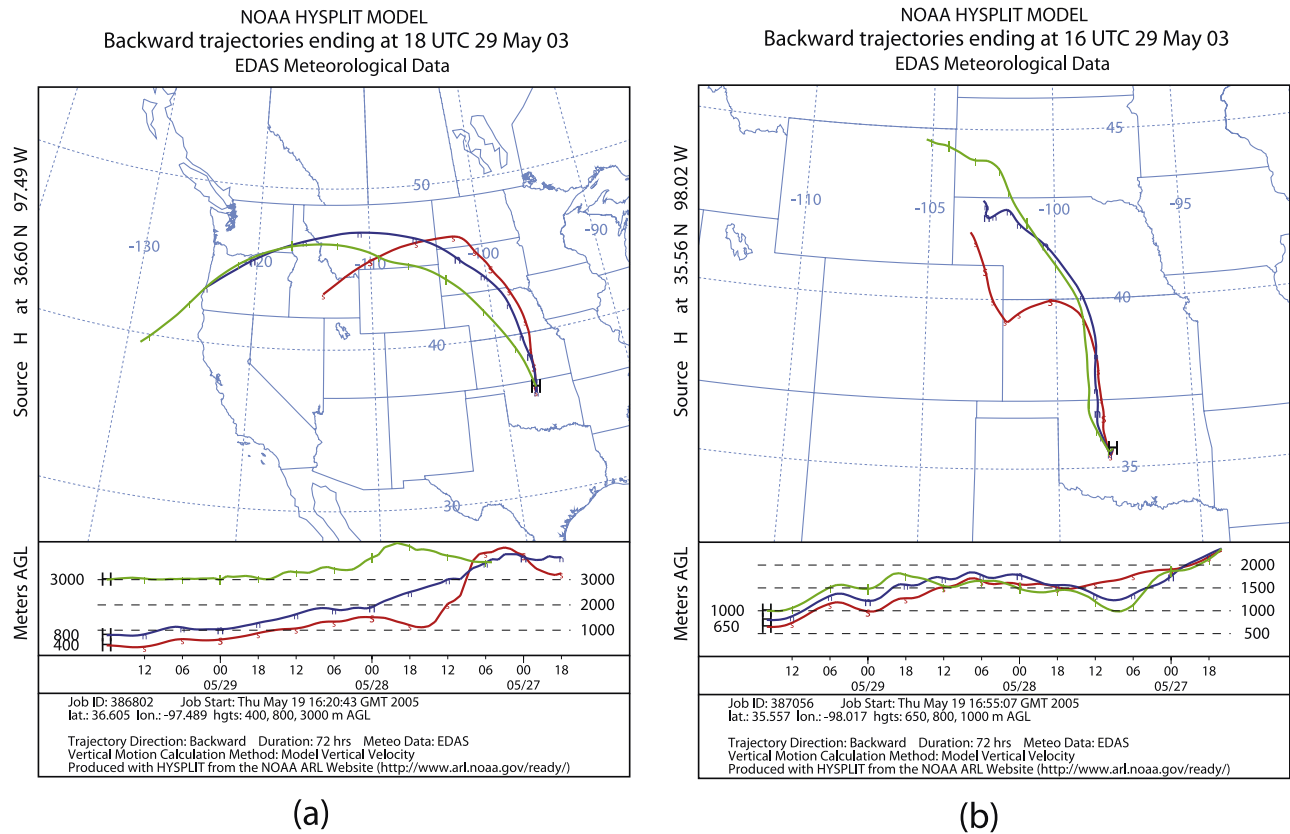
Figure 10. Three-day HYSPLIT back trajectories for 29 May 2003 (flight 17) (a) at the SGP site at altitudes of 400, 800, and 3000 m and (b) at site EF-19 at altitudes of 650, 800, and 1000 m. The times given are UTC; 1700 UTC corresponds to 1200 LT.

common [*Pruppacher and Klett*, 1997]. Lower insoluble fractions would be expected in the ambient aerosol, especially if the aerosol were truly internally mixed independently of particle size. Under the assumption of a size-independent internal mixture of particles, the values of ε_{ins} that would be required to achieve agreement between N_P and N_O exceed the average fraction of insoluble material commonly found in continental aerosols. Other aerosol properties likely contributed to the discrepancy between N_P and N_O.

5.2.2. CCN and DACAD Derived Insoluble Fraction (Flight 10)

[39] During the IOP, there was one flight (flight 10) during which CCN concentrations and DACAD wet and dry aerosol size distributions were all measured. From the wet and dry aerosol size distributions and assuming size-independent internally mixed aerosol population, an estimate of ε_{ins} can be obtained by comparing the cumulative particle concentrations of the wet and dry size distributions at each diameter. The average difference in wet and dry

Table 3. Insoluble Volumetric Fractions (ε_{ins}) and Fraction of Particles Unavailable for Activation (f_{NA}) for Which $\mu(N_P/N_O) \approx 1$

s, %	d_{act}, nm	Flight	ε_{ins}[a] (Range[b])	ε_{ins}[a] (Mean[c])	f_{NA}[d] (Range[b])	f_{NA}[d] (Mean[c])
2.8	15	6	0.66–0.96	0.90	0–0.39	0.22
2.8	15	7	0.93–0.96	0.94	0–0.27	0.21
2.8	15	8	0.97–>0.99	0.98	0.13–0.37	0.15
2.8	15	10	>0.99 (all)	>0.99	0.24–0.26	0.25
3.6	13	9	0.91–>0.99	0.98	0.04–0.61	0.22
2.1	18	12	0.78–0.96	0.92	0.26–0.64	0.42
2.1	18	13	0.95–0.98	0.96	0.17–0.61	0.40
2.1	18	14	0.98–>0.99	>0.99	0.24–0.63	0.42
2.1	18	15	0.92–>0.99	0.98	0.36–0.70	0.44
2.1	18	16	>0.99 (all)	>0.99	0.40–0.91	0.63
2.1	18	17	0.87–>0.99	0.98	0.50–0.76	0.69

[a]Size-independent internal mixing is assumed in the determination of ε_{ins}.
[b]The ranges of values for ε_{ins} and f_{NA} are determined from those averaged over each of the level legs during a flight.
[c]The mean values of ε_{ins} and f_{NA} are averaged over all analysis points.
[d]N_P is determined under the assumption of pure $(NH_4)_2SO_4$ in the determination of f_{NA}.

Table 4. Flight 10 Analysis Using $\varepsilon_{ins} = \varepsilon_{ins,DACAD}$ as Determined From DACAD Wet and Dry Cumulative Size Distributions

DACAD Midscan Time	$\varepsilon_{ins,DACAD}$	$D_c{}^a(\varepsilon_{ins,DACAD})$, nm	$N_P(D_c)$, cm^{-3}	N_O, cm^{-3}	N_P/N_O	$f_{NA}{}^b$
1630:11	0.88	30	769	618	1.24	0.20
1632:28	0.71	22	797	530	1.50	0.34
1633:51	0.85	26	743	579	1.28	0.22
1635:05	0.76	22	743	588	1.26	0.21
1637:32	0.75	22	759	578	1.31	0.24
1638:45	0.74	22	665	564	1.18	0.15
1642:26	0.94	36	655	490	1.34	0.25
1643:39	0.92	30	620	512	1.21	0.18
1657:07	0.84	26	2093	1720	1.22	0.18
1658:20	0.89	30	1915	1621	1.18	0.15
1659:34	0.78	26	1858	1454	1.28	0.22
1700:47	0.86	26	1728	1331	1.30	0.23
1702:01	0.83	26	1586	1292	1.23	0.19
1703:14	0.75	22	1483	1162	1.28	0.22
1704:28	0.72	22	1475	1204	1.22	0.18
1705:41	0.80	26	1334	1116	1.20	0.16
1711:49	0.72	22	1505	1148	1.31	0.24
1713:02	0.77	26	1740	1288	1.35	0.26
1714:16	0.83	26	1874	1404	1.33	0.25
1715:29	0.72	22	1895	1422	1.33	0.25
1725:17	0.69	22	700	538	1.30	0.23
1726:31	0.36	19	707	535	1.32	0.24
1730:11	0.73	22	697	526	1.32	0.25

[a]D_c is the cutoff diameter of a particle with insoluble fraction $\varepsilon_{ins,DACAD}$ and the balance $(NH_4)_2SO_4$ at 2.8% supersaturation.
[b]The f_{NA} values are determined using $\varepsilon_{ins} = \varepsilon_{ns,DACAD}$.

diameter between the wet and dry cumulative concentration curves can give an estimate of the hygroscopic growth factor $(G(RH)_{Total})$ of the aerosol population during the scan in question. $G(RH)_{Total}$ is used instead of the hygroscopic growth factor, $f(RH)$, because $G(RH)_{Total}$ is based on the difference between the wet and dry diameters of the particle, which is directly related to the water uptake by the particle and is more directly applicable to CCN activity. The total growth factor can be used to estimate ε_{ins} from,

$$G(RH)_{Total}^3 = \varepsilon_{ins} + \varepsilon_{org}G(RH)_{org}^3 + \varepsilon_{sol}G(RH)_{sol}^3 \quad (1)$$

where ε_{org} is the volumetric fraction of organic material, $G(RH)_{org}$ is the growth factor of organic material, ε_{sol} is the volumetric fraction of soluble material, and $G(RH)_{sol}$ is the growth factor of soluble material. If it is assumed that no soluble organic material is present in the aerosol particles, then the calculated value of ε_{ins} will be the maximum fraction of insoluble material possible for the determined value of $G(RH)_{Total}$. Then, equation (1) can be solved for $\varepsilon_{ins,DACAD}$, the insoluble fraction estimated from the DACAD wet and dry aerosol size distributions,

$$\varepsilon_{ins,DACAD} = \frac{G(RH)_{Total}^3 - G(RH)_{sol}^3}{1 - G(RH)_{sol}^3} \quad (2)$$

The soluble particle fraction is assumed to be composed of deliquesced $(NH_4)_2SO_4$, for which the value of $G(RH)_{sol}$ is 1.35 at the approximate DACAD operating RH of 70%.

[40] The average value of the growth factor for the aerosol populations during flight 10, $G(RH)_{ave}$, is 1.05, and the average $\varepsilon_{ins,DACAD}$ is 0.78. The $G(RH)_{Total}$ and $\varepsilon_{ins,DACAD}$ values for each DACAD scan, and the result-

ing $\mu(N_P/N_O)$, are given in Table 4. N_P is the summation of particles from the DACAD size distribution that have diameters greater than a cutoff diameter, D_C, which is the activation diameter (at 2.8% supersaturation) of a particle with an insoluble fraction equal to $\varepsilon_{ins,DACAD}$ and with the balance $(NH_4)_2SO_4$. DACAD scans with $G(RH)_{Total}$ less than unity, and thus $\varepsilon_{ins,DACAD}$ values greater than unity, were eliminated from this analysis. A value of $G(RH)_{Total}$ less than unity could result when the assumption of size-independent internal mixing is invalid or for scan times during which the aerosol population is changing rapidly and the DACAD is unable to resolve these changes.

[41] The values of $\varepsilon_{ins,DACAD}$ derived from the DACAD size distributions for flight 10 still result in $\mu(N_P/N_O)$ values greater than unity, which indicates, in accord with the previous analysis, that even a maximum estimate of ε_{ins} is not sufficient to obtain agreement between N_P and N_O in this continental environment. Other properties of the aerosol population need to be considered when attempting to obtain satisfactory agreement between N_P and N_O. The next property to consider is the mixing state of the aerosol population.

5.3. Inverse Aerosol/CCN Closure: Inferring Aerosol Mixing State
5.3.1. Aerosol Mixing State Inferred From Initial Comparison of N_P and N_O

[42] The aerosol mixing state can be inferred from the initial comparison of N_P and N_O (section 5.1) in an inverse analysis similar to that carried out for the insoluble volume fraction. In this mixing state analysis, N_P is calculated by assuming pure $(NH_4)_2SO_4$ particles. The fraction of particles that is unavailable for activation (f_{NA}) could consist of purely insoluble particles or particles with an insoluble fraction that is large enough to prevent activation. The f_{NA}

such that $\mu(N_P/N_O) \approx 1$ is calculated from the following equation,

$$f_{NA} = \frac{N_{PExt}}{N_P} = \frac{N_P - N_O}{N_P} = 1 - \frac{N_O}{N_P} \qquad (3)$$

where N_{PExt} is the number concentration of the externally mixed particles that are unavailable for activation. The statement that $N_{PExt} = N_P - N_O$ assumes that the CCNC3 was able to count all particles that were capable of activating at the operating supersaturations, which is likely at such high supersaturations where kinetic effects would not be dominant. Table 3 gives the average f_{NA} for each flight and the results are discussed further in section 5.3.3.

5.3.2. Aerosol Mixing State Inferred With DACAD Derived Insoluble Fraction (Flight 10)

[43] Along with the $\varepsilon_{ins,DACAD}$ estimates, which were not sufficient to obtain agreement between N_P and N_O, an additional estimate of the extent of external mixing of the aerosol population can be calculated for flight 10. For this analysis, the f_{NA} that leads to $\mu(N_P/N_O) \approx 1$ is calculated by considering $\varepsilon_{ins,DACAD}$ (constant for particles of all diameters) with the balance $(NH_4)_2SO_4$ in the calculation of N_P. Table 4 shows the values of f_{NA} that satisfy $\mu(N_P/N_O) \approx 1$ for each DACAD scan during flight 10. The average value of f_{NA} in Table 4 is 0.22, which is close to the average value of f_{NA} (0.25) for flight 10 with $\varepsilon_{ins} = 0$. The similar values of f_{NA} calculated with and without the maximum value of ε_{ins} for a size-independent internal mixture of particles ($\varepsilon_{ins,DACAD}$) indicates that the aerosol was an external mixture that included some purely insoluble particles. Particles with an insoluble fraction of $\varepsilon_{ins,DACAD}$ that were unable to activate at the operating supersaturations of the CCNC3 made up only 3% of the total aerosol population; 22% were purely insoluble particles (that did not activate), and 78% of the particles were able to activate.

5.3.3. Aerosol Mixing State Discussion

[44] The values of f_{NA} follow a similar trend to that seen for $\mu(N_P/N_O)$ in section 5.1, with more particles unavailable for activation during flights that encountered polluted conditions. The aerosol size distribution feature that distinguishes between polluted and clean conditions is the predominance of small particles with diameters less than 30 nm under polluted conditions. The increase in f_{NA} values with increasing polluted conditions, therefore, indicates that the particles that are unavailable for activation at the operating supersaturations of the CCNC3 are predominantly those with diameters less than 30 nm. This is consistent with the findings of *Gasparini et al.* [2006], that the smallest analyzed particles were largely composed of nonhygroscopic compounds (see section 4.1). At the relatively high operating supersaturations of the CCNC3, these small (<30 nm), largely nonhygroscopic particles would make up the majority of the particles that remained unactivated. Considering that the insoluble fractions in a size-independent internal mixture required for N_P and N_O agreement in section 5.2 exceed 0.90 for 99 out of the 113 level legs analyzed, f_{NA} probably consists of some pure insoluble particles, with a range of diameters. An internal mixture of particles with an even distribution of insoluble material across particle diameters is not expected, especially at the

location of the SGP site, where sampled aerosol varies in both source and age.

5.4. CCN and DMA/TDMA Derived Mixing State and Particle Composition

[45] Size-resolved particle composition and mixing state of ambient aerosol were derived from the Texas A&M DMA/TDMA ground data from the IOP [*Gasparini et al.*, 2006]. For each size bin, the DMA/TDMA measurements can be used to calculate the fraction of the particles in that size bin that are purely soluble material, purely insoluble material, and a mixture of soluble and insoluble material. The fraction of insoluble material in the mixed particles is also calculated. It was assumed that the purely insoluble particles did not activate at the operating supersaturations of the instrument. The purely soluble particles were assumed to activate if the size bin diameter was greater than the critical diameter of $(NH_4)_2SO_4$ at the operating supersaturation of the CCNC3 instrument. The mixed particle soluble and insoluble fractions were input into the Köhler model to determine whether particles with this chemical composition and diameters equal to the middiameter of the size bin were able to activate at the operating supersaturation of the CCNC3 instrument.

[46] The flights for which there were simultaneous CCN measurements, DACAD size distributions, and DMA/TDMA-derived aerosol population properties were flights 8, 9, and 16. For this analysis, included level legs were limited to being within 8047 m (5 miles; horizontal distance) of the SGP CART site and within the boundary layer, where the ground DMA/TDMA-derived aerosol properties are more likely to be valid for flight data. The boundary layer height was calculated using the procedure described by *Delle Monache et al.* [2004], which uses Balloon-Borne Sounding System data. The boundary layer height is defined as the lowest altitude within a potential temperature inversion at which a critical lapse rate and threshold potential temperature are exceeded. The following thresholds were determined by *Delle Monache et al.* [2004] to apply at the SGP CF: $\theta_{Top} - \theta_{Bottom} = 2$ K and $\Delta\theta/\Delta z = 0.001$ K m^{-1}, where θ_{Top} is the potential temperature at the top of the boundary layer in Kelvin (K), θ_{Bottom} is the potential temperature at the bottom of the boundary layer in K, θ is the potential temperature in K, and z is the altitude in m. DMA/TDMA data were used to classify aerosol particle components as externally mixed insoluble, externally mixed soluble, internally mixed insoluble, and internally mixed soluble, and these aerosol properties were averaged over the diameter ranges of the DACAD. DACAD scan times within the DMA/TDMA size distribution scan times (~5 min) were used.

[47] The $\mu(N_P/N_O)$ values resulting from the DMA/TDMA-derived properties are given in Table 5. For flights 8 and 9, the $\mu(N_P/N_O)$ values are within instrument uncertainty, but they are still significantly greater than unity for flight 16, even though using the DMA/TDMA-derived aerosol properties decreased the $\mu(N_P/N_O)$ value significantly, by about 73%. The flight traces for flights 8 and 9 (Figures 11 and 12) show well-mixed boundary layers for the time periods during which the Twin Otter was sampling within the boundary layer and within 8 km of the ground site. The boundary layer during the time period studied for

Table 5. $\mu(N_P/N_O)$ and $\sigma(N_P/N_O)$ Values for Flights 8, 9, and 16 Using ε_{ins} and External Mixing Properties Derived From DMA/TDMA Data[a]

|				Without DMA/TDMA Derived Properties ($\varepsilon_{ins} = 0$, $f_{NA} = 0$)		With DMA/TDMA Derived Properties	
s, %	d_{act}, nm	Flight	Number of DACAD Scans Included	$\mu(N_P/N_O)$	$\sigma(N_P/N_O)$	$\mu(N_P/N_O)$	$\sigma(N_P/N_O)$
2.8	15	8	4	1.18	0.02	1.00	0.02
3.6	13	9	1	1.14	one scan	1.10	one scan
2.1	18	16	3	5.38	2.26	1.47	0.15

[a]The results without DMA/TDMA derived properties are also given for the same DACAD scans. This table only includes times during which the Twin Otter was within 5 miles of the SGP CART site and within the boundary layer.

flight 16 is less well mixed, as is illustrated by its flight trace in Figure 13. The time period within which the Twin Otter was sampling within the boundary layer and within 8 km of the ground site was near the beginning of flight 16, from about 1849 to 1851 UTC. Considering that the DMA/ TDMA data were measured at the ground, it is not unexpected that the agreement between N_P and N_O is more satisfactory for well-mixed boundary layers than non-well-mixed boundary layers.

[48] A comparison of the DMA/TDMA and DACAD aerosol size distributions illustrates this point further. Figure 14 compares the DMA/TDMA and DACAD aerosol and predicted CCN size distributions for flights 8 and 9; Figure 15 illustrates the same for flight 16. Both of the CCN size distributions (DMA/TDMA and DACAD) are calculated using the size-resolved chemistry derived from the DMA/TDMA measurements. For the DACAD CCN size distributions, the DMA/TDMA size-resolved chemistry is applied to the DACAD aerosol size distributions, which assumes that the DMA/TDMA-derived chemistry applies at the sampling altitude of the

DACAD. As can be seen, this assumption seems to hold for flights 8 and 9 but not flight 16.

[49] During the sampling period 1849 to 1851 UTC during flight 16, the CPC and DACAD exhibit sharp peaks in number concentration. The DACAD aerosol size distribution shows that these peaks are caused by increases in small particles that do not show up in the DMA/TDMA size distribution for the same time period. This indicates that the layers that were sampled by the Twin Otter did not necessarily reach the ground and that the aerosol layers within the boundary layer were stratified. The DELTA (Detection and Evaluation of the Long-Range Transport of Aerosols) rotating drum impactor aerosol composition results from the SGP site measurements also indicate that the layers sampled aloft on 25–29 May did not reach the ground [Cahill et al., 2004]. Another possibility is that the DMA/TDMA, which has a longer total sequence scan time (∼1 hour) than the DACAD (72.5 s), was unable to resolve rapid changes in the aerosol size distribution, which may have occurred during the time period of interest. The DMA/TDMA size-
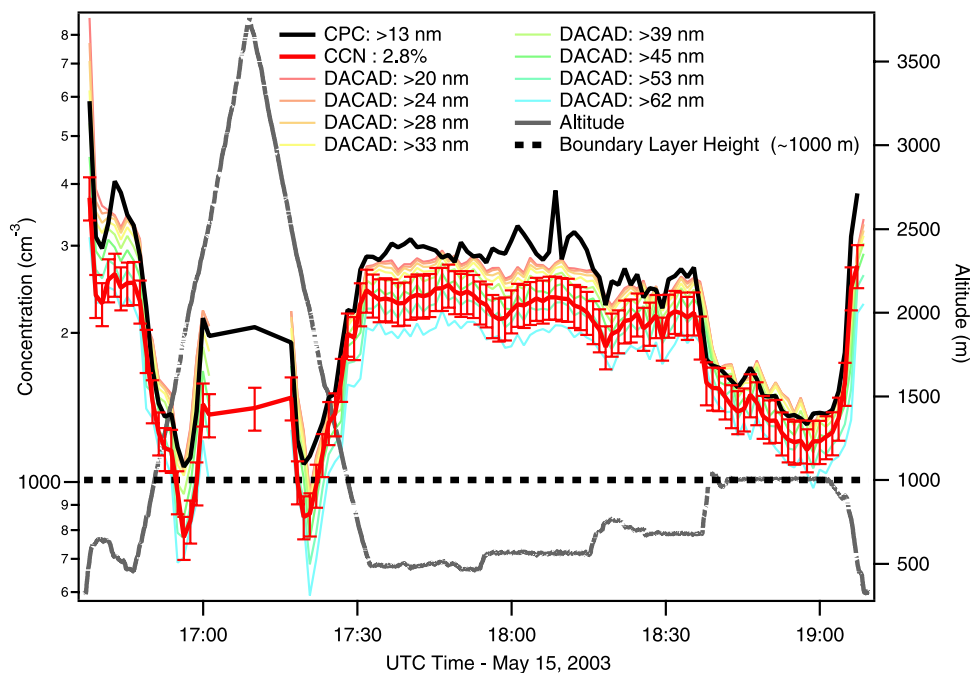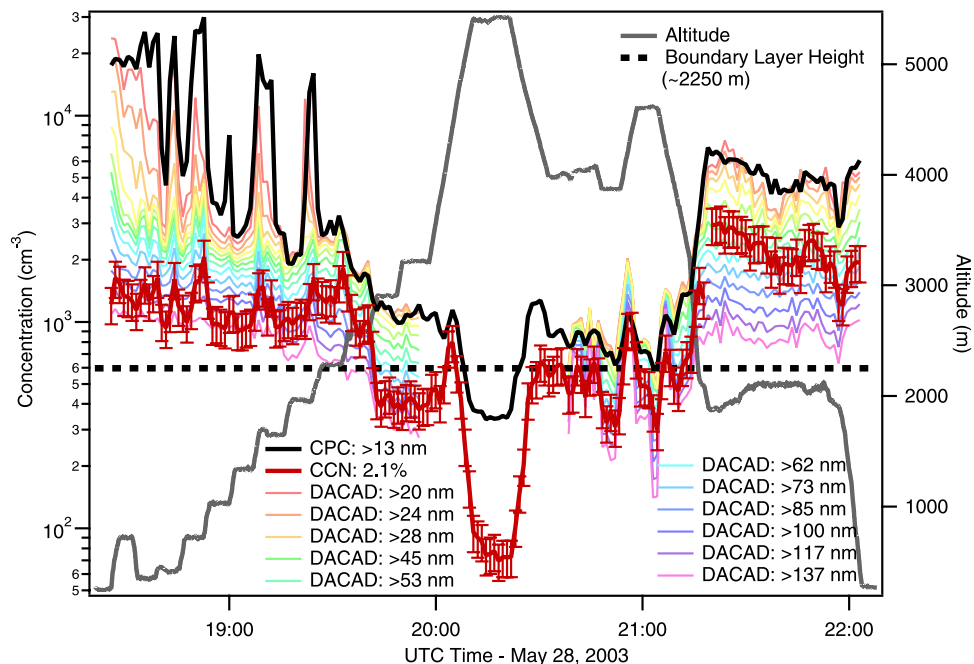

Figure 11. Flight trace for flight 8, showing a well-mixed boundary layer between approximately 1730 and 1840 UTC when the Twin Otter was sampling beneath ∼1000 m. The error bars on the CCN trace indicate the 10% uncertainty level. The times given are UTC; 1700 UTC corresponds to 1200 LT.
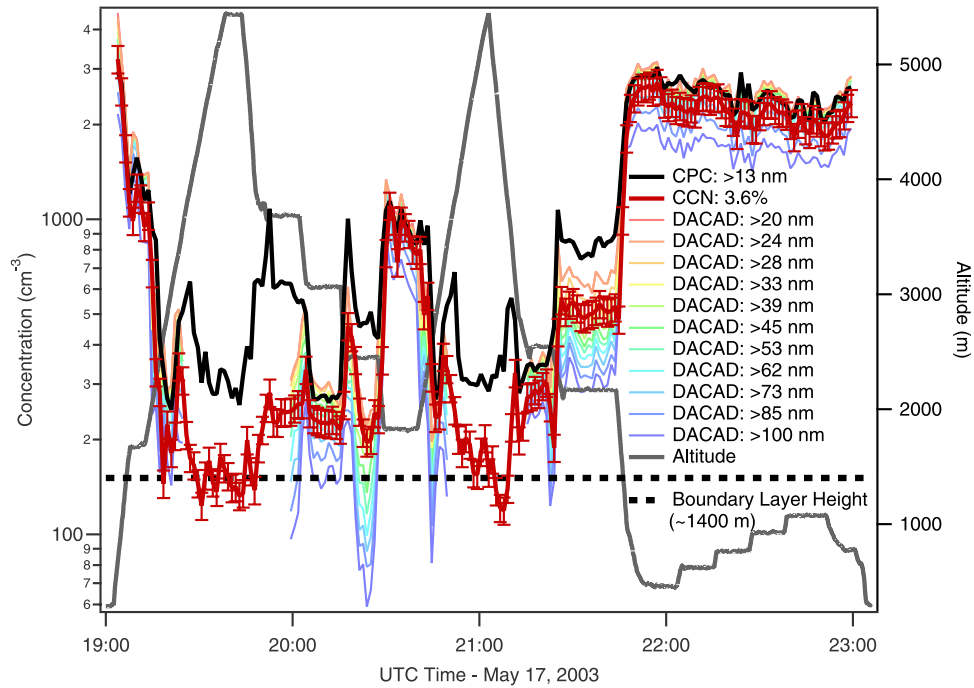
Figure 12. Flight trace for flight 9, showing a well-mixed boundary layer between approximately 2200 and 2300 UTC when the Twin Otter was sampling beneath ~1400 m. The error bars on the CCN trace indicate the 10% uncertainty level. The times given are UTC; 1700 UTC corresponds to 1200 LT.

resolved composition does not apply to the air masses sampled by the Twin Otter for flight 16 because the shape of the DMA/TDMA and DACAD sampled aerosol size distributions are not similar. If the DMA/TDMA and DACAD size distribution shapes are similar, as is true for flights 8 and 9, then the DMA/TDMA composition results can be coupled with airborne aerosol size distribution measurements to predict CCN concentrations with-

Figure 13. Flight trace for flight 16, showing the lack of a well-mixed boundary layer from approximately 1820 to 1940 UTC when the Twin Otter was sampling beneath ~2250 m. The error bars on the CCN trace indicate 20% uncertainty level. The times given are UTC; 1700 UTC corresponds to 1200 LT.
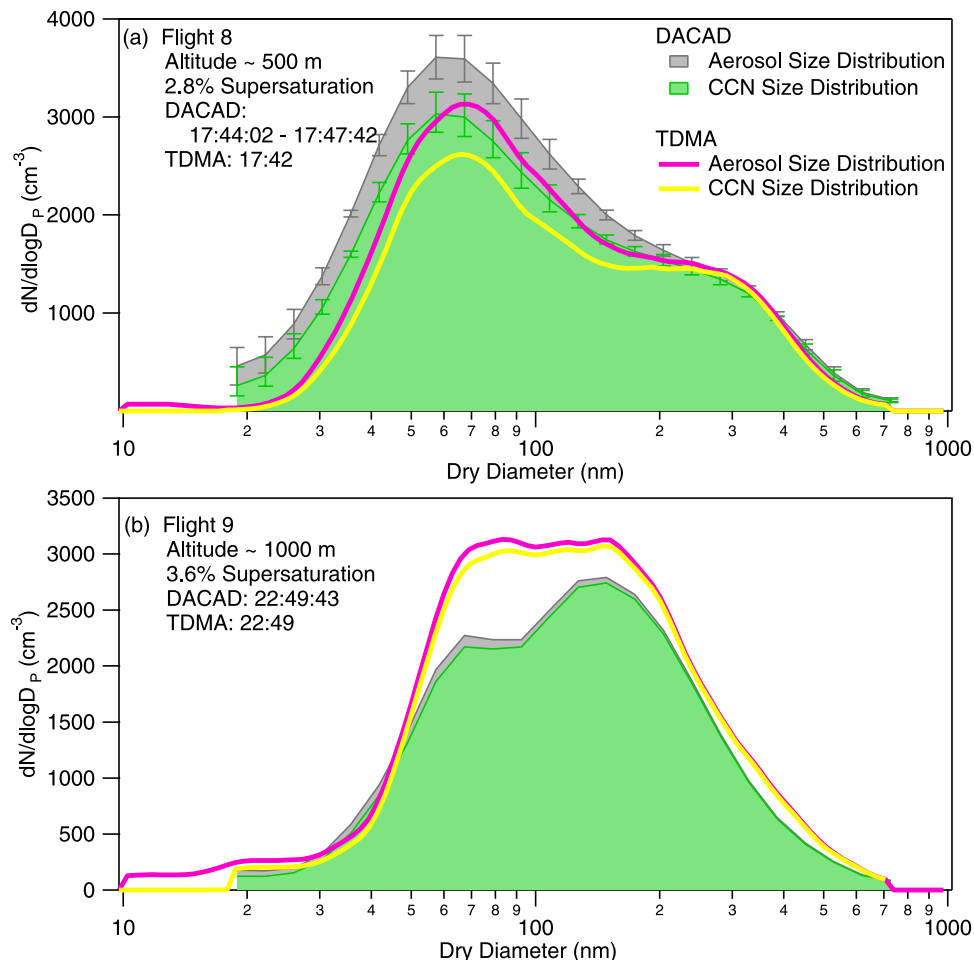
Figure 14. Comparison of DMA/TDMA and DACAD size distributions for flights (a) 8 and (b) 9. The error bars give the standard deviation of the DACAD aerosol size distributions averaged over the DMA/TDMA scan times. The times given are DACAD midscan times in UTC; 1700 UTC corresponds to 1200 LT. The area under the aerosol size distribution curve gives the total aerosol number concentration, and the area under the CCN size distribution curve gives the predicted CCN number concentration. Both DACAD and DMA/TDMA predicted CCN distributions were calculated using the insoluble fraction and external mixing properties determined from the DMA/TDMA data.

in the boundary layer and within a reasonable horizontal distance from the ground measurement site.

6. Case Studies: "Clean" Conditions, Local Pollution, and Siberian Smoke Events

[50] The inverse aerosol/CCN closure study (assuming 100% $(NH_4)_2SO_4$) indicates a division of the flights into three groups, based on the value of the closure ratio of N_P to N_O. Flights 6 through 10 (14–18 May) have $\mu(N_P/N_O)$ values between 1.18 and 1.34, while values for flights 12 through 15 (21–27 May) are between 1.78 and 1.87, and values for flights 16 and 17 (28 and 29 May) are 3.68 and 3.45, respectively. This division seems independent of the instrument operating supersaturation. Operating supersaturations of 2.8% and 3.6% are included in flights 6 through 10, which have similar $\mu(N_P/N_O)$ values. The operating supersaturation (2.1%) is the same for flights 12 through 17, although each flight has different $\mu(N_P/N_O)$ values. ARM Aerosol IOP flights fall into categories consistent

with relatively clean conditions with intermittent pollution events (flights 6–10), conditions influenced by local pollution and/or smoke events (flights 12–15), and conditions dominated by local pollution events (flights 16–17) [Schmid et al., 2004]. Aerosol size distributions from the DACAD are especially illustrative of the different categories of sampled air masses. In the following discussions, only DACAD scan times that were used in the inverse closure analysis are considered and presented.

[51] During the first two weeks of the ARM Aerosol IOP (5–18 May, flights 6–10), relatively clean atmospheric conditions were noted. Also during this time, severe weather moved through north-central Oklahoma, including a "thunderstorm and high wind" event on 16 May (NOAA National Climatic Data Center (NCDC) access via Department of Commerce (DOC) NOAA National Environmental Satellite, Data, and Information Service (NESDIS) NCDC website, http://lwf.ncdc.noaa.gov/oa/ncdc.html). This may be one reason that the atmosphere was relatively clean. DACAD size distributions early in flights 6–10 (14–
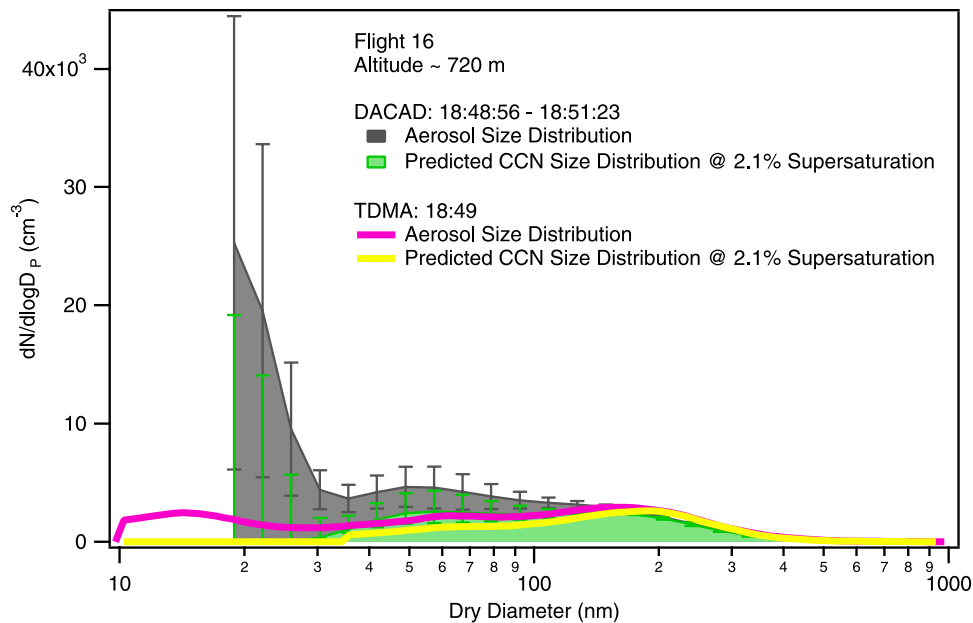
Figure 15. Comparison of DMA/TDMA and DACAD size distributions for flight 16. The error bars give the standard deviation of the DACAD aerosol size distributions averaged over the DMA/TDMA scan times. The times given are the DACAD midscan times in UTC; 1700 UTC corresponds to 1200 LT. The area under the aerosol size distribution curve gives the total aerosol number concentration, and the area under the CCN size distribution curve gives the predicted CCN number concentration. Both DMA/TDMA and DACAD predicted CCN distributions were calculated using the insoluble fraction and external mixing properties determined from the DMA/TDMA data.

18 May) have unimodal or bimodal distributions with median diameters between about 40 and 160 nm and peak $dN/dlogD_P$ values less than 5000 cm^{-3}. Aerosol size distributions for flight 6 begin to deviate from these characteristics about 45 min after takeoff and continue to deviate until landing. Aerosol size distributions exhibit these ''clean'' characteristics throughout the analyzed times during flights 7, 8 and 10. For flight 9, aerosol size distributions exhibit these ''clean'' characteristics near the end, as well as early in, the flight, but deviate for midflight times. The $\mu(N_P/N_O)$ values for these clean background periods are 1.19, 1.33, 1.18, 1.21, and 1.34 for flights 6–10, respectively.

[52] Background closure ratios for flights 9 and 10 (1.21 and 1.34, respectively) on 17 and 18 May may include data points related to a sulfur event in the SGP area. Around 17 May, *Cahill et al.* [2004] noted, on the basis of their ground site data, an aerosol sulfur episode caused by an air mass that they predict was over Ohio 2 days earlier. Most of the aerosol size distributions from flights 9 and 10 are unimodal with median diameters greater than 100 nm, which could be indicative of an aged aerosol population and which is consistent with the findings of *Cahill et al.* [2004]. Some aerosol size distributions from flight 9 indicate the influence of local aerosol sources, as will be discussed.

[53] After 18 May, the aerosol size distributions are unimodal or bimodal with median diameters between 40 and 80 nm and peak $dN/dlogD_P$ values less than 10,000 cm^{-3}. Aerosol size distributions with these ''dirtier'' background aerosol characteristics were found during

flights 12–17 (21–29 May). The $\mu(N_P/N_O)$ values for background conditions during flights 12–17 are 1.36, 1.28, 1.70, 1.54, 2.30, and 2.30, respectively.

[54] At later times during flight 6, midtimes during flight 9, and times throughout flights 12–17, measured aerosol size distributions indicated the presence of local pollution sources. Elevated aerosol layers were visually observed at altitudes of ~3700 m during flight 6, ~2500 m during flight 9, ~3000 and 3700 m during flight 14, and ~2000, 3000, 3700, and 5000 m during flight 15. Some DACAD size distributions from flights 6, 7, 9, and 12–17 have characteristically low median diameters (sometimes less than the cutoff diameter of the DACAD, ~17 nm) and particularly large concentrations of particles with diameters less than 30 nm. These aerosol size distributions are consistent with those from locations that are downwind of a fresh pollution source, such as a coal-fired power plant [*Brock et al.*, 2002]. Ground-based PILS-IC results show that for flights 12, 14, and 15 (21, 25, and 27 May) NH$_4^+$ to SO$_4^{-2}$ molar ratios much less than 2 were observed [*Pahlow et al.*, 2006], which could indicate addition of sulfate to particles through vapor and aqueous phase reactions. The SGP site is near two power plants: the Ponca City and Conoco power plants, and IOP flight patterns passed near at least four other industrial and/or power plants, as well. Figure 1 shows the locations of these plants. The $\mu(N_P/N_O)$ values for these periods that seem to be influenced by local pollution are 1.35 and 1.26 for flights 6 and 9, respectively and 1.89, 1.85, 2.41, 2.73, 6.83, 3.75 for flights 12–17, respectively.

Table 6. Summary of the Values of $\mu(N_P/N_O)$ for Each Flight, Divided Into Categories Determined From DACAD Size Distributions[a]

			$\mu(N_P/N_O)$		
s, %	d_{act}, nm	Flight	Background	Polluted	Smoke
2.8	15	6	1.19	1.35	NE
2.8	15	7	1.33	NE	NE
2.8	15	8	1.18	NE	NE
2.8	15	10	1.34	NE	NE
3.6	13	9	1.21	1.26	NE
2.1	18	12	1.36	1.89	NE
2.1	18	13	1.28	1.85	NE
2.1	18	14	1.70	2.41	2.28
2.1	18	15	1.54	2.73	1.61
2.1	18	16	2.30	6.83	NE
2.1	18	17	2.30	3.75	NE

[a]"NE" indicates that the condition was "not encountered" during the DACAD scan times used in the closure analysis.

[55] Table 6 summarizes the $\mu(N_P/N_O)$ values for all flights when divided into categories based on the shape and magnitude of the DACAD aerosol size distribution. In general, the $\mu(N_P/N_O)$ values are lower for the clean conditions than the more obviously polluted conditions.

[56] Siberian smoke layers were observed in the SGP CF area during the period 25–28 May, 2003 (flights 14–17) [*Schmid et al.*, 2004]. DACAD aerosol size distributions indicate that smoke layers were sampled at altitudes of ~3700 m on flight 14 and ~3100 m on flight 15. The Siberian fires were detected in April but escalated greatly in May. In transport simulations beginning on 10 May 2003, the smoke plume from Siberia reached Canada in about 11 days, with a smoke maximum on 23 May in Manitoba, Canada [*Damoah et al.*, 2004]. HYSPLIT [*Draxler and Rolph*, 2003; *Rolph*, 2003] back trajectories for flight 14 on 25 May 2003 show that air masses 3000 and 4000 m over the ARM SGP site were over Canada 2 days prior to sampling, which corresponds with the smoke maximum in Manitoba on 23 May.

[57] On 25 May 2003 (flight 14), the observed elevated layers were characterized by large values of dry extinction and backscatter, which are consistent with aged smoke particles [*Ghan et al.*, 2006]. The DACAD size distributions from these smoke events tend to have a large accumulation mode, with median diameters greater than 100 nm. This is consistent with aged aerosol populations originating from biomass burning, in which processes such as particle coagulation and cloud processing have occurred and have decreased the peak concentration and increased the median diameter of the size distribution [*Radke et al.*, 1995].

[58] The ability of smoke particles to act as CCN has been shown to increase with smoke plume age [*Andreae and Merlet*, 2001]. The critical supersaturation of smoke particles is reduced, and thus their CCN ability increased, through cloud processing, in which condensational uptake of water-soluble material is possible. Past studies have found that the ratio of CN to CCN at 1% supersaturation is about 1.7 in a slightly aged (1–2 hours) smoke plume [*Andreae and Merlet*, 2001]. The Siberian smoke aerosols were transported over a large distance, which included time spent over industrial and desert regions. Therefore, along with aged smoke particles, it is likely that industrial

pollutants and some mineral dust were present in these smoke layers [*Jaffe et al.*, 2004]. This may explain why the $\mu(N_P/N_O)$ values, given in Table 6, differ from those of other studies of aged smoke plumes.

[59] The layers that were analyzed in the closure analysis for flights 16 and 17 have aerosol size distributions that are more consistent with local pollution sources than with aged smoke particles. Flight 17 was a MODIS overpass flight, which sampled above three ARM ground sites, in addition to the SGP CF. During flight 17, the Twin Otter flew near five power plants, so the aerosol size distribution characteristics are not unexpected.

7. Conclusions

[60] The inverse aerosol/CCN closure study has revealed possible features of the aerosol sampled during the ARM Aerosol IOP in the absence of direct airborne aerosol composition measurements. The ARM SGP site is greatly influenced by local aerosol sources, as well as long-range sources, and the aerosol CCN activity at high supersaturations was greatly influenced by the chemical characteristics and mixing state of the aerosols in the sampled air masses. The characteristics of air masses sampled during the ARM Aerosol IOP ranged from those of relatively clean air masses to those of air masses influenced by local and long-range pollution events to those of aged smoke plumes. These air masses can be categorized by aerosol size distribution, as well as by CCN behavior as indicated in the ratio of N_P to N_O. It has been shown that the general low aerosol CCN activity that was observed in this inverse aerosol/CCN study is consistent with other measurements from the IOP.

[61] The DACAD aerosol size distributions measured during the ARM Aerosol IOP were highly variable, even on level legs of approximately constant altitude. This could account for some of the disagreement between N_P and N_O because the DACAD is not able to resolve rapid changes in aerosol size distributions because of its longer measurement time compared to that of the CCNC3.

[62] If the CCNC3 instrument had operated at lower supersaturations that are more representative of those found in the atmosphere, the inverse aerosol/CCN closure study may have resulted in significantly different N_P to N_O ratios. The only indication that we have of the size resolved aerosol composition in this area is the DMA/TDMA derived results. These results indicate that, in general, material of low hygroscopicity was preferentially distributed among the smallest measured particles. This is consistent with in-cloud aerosol processing and/or fresh pollution sources, and it is likely that both of these scenarios were encountered during the ARM Aerosol IOP because of the close proximity of power and industrial plants and the verified Siberian smoke events near the end of the month.

[63] Although some of the chemistry effects may not have been captured at smaller supersaturations, future measurements should be made at lower operating supersaturations to better determine the ability to predict CCN concentration using surface data. However, for a continental location such as the ARM SGP site that is influenced by many different aerosol sources, ranging from local to international, predicting CCN concentrations from aerosol size distributions and surface aerosol composition measurements alone is proba-

bly not adequate. Future studies should also include airborne aerosol composition measurements to allow more complete aerosol/CCN closure studies.

References

Albrecht, B. A. (1989), Aerosols, cloud microphysics, and fractional cloudiness, *Science*, 245(4923), 1227–1230.

Andreae, M. O., and P. Merlet (2001), Emission of trace gases and aerosols from biomass burning, *Global Biogeochem. Cycles*, 15(4), 955–966.

Brechtel, F. J., and S. M. Kreidenweis (2000a), Predicting particle critical supersaturation from hygroscopic growth measurements in the humidified TDMA. Part I: Theory and sensitivity studies, *J. Atmos. Sci.*, 57(12), 1854–1871.

Brechtel, F. J., and S. M. Kreidenweis (2000b), Predicting particle critical supersaturation from hygroscopic growth measurements in the humidified TDMA. Part II: Laboratory and ambient studies, *J. Atmos. Sci.*, 57(12), 1872–1887.

Brock, C. A., et al. (2002), Particle growth in the plumes of coal-fired power plants, *J. Geophys. Res.*, 107(D12), 4155, doi:10.1029/2001JD001062.

Cahill, T. A., L. Portnoff, and R. A. Reck (2004), Impact of long-range aerosol transport in Oklahoma, May 2003, paper presented at Fourteenth ARM Science Team Meeting, U.S. Dep. of Energy, Albuquerque, N. M.

Carrico, C. M., M. J. Rood, and J. A. Ogren (1998), Aerosol light scattering properties at Cape Grim, Tasmania, during the first Aerosol Characterization Experiment (ACE 1), *J. Geophys. Res.*, 103(D13), 16,565–16,574.

Chuang, P. Y., A. Nenes, J. N. Smith, R. C. Flagan, and J. H. Seinfeld (2000), Design of a CCN instrument for airborne measurement, *J. Atmos. Oceanic Technol.*, 17(8), 1005–1019.

Covert, D. S., R. J. Charlson, and N. C. Ahlquist (1972), A study of the relationship of chemical composition and humidity to light scattering by aerosols, *J. Appl. Meteorol.*, 11(6), 968–976.

Damoah, R., N. Spichtinger, C. Forster, P. James, I. Mattis, U. Wandinger, S. Beirle, T. Wagner, and A. Stohl (2004), Around the world in 17 days—Hemispheric-scale transport of forest fire smoke from Russia in May 2003, *Atmos. Chem. Phys.*, 4, 1311–1321.

Delle Monache, L., K. D. Perry, R. T. Cederwall, and J. A. Ogren (2004), In situ aerosol profiles over the Southern Great Plains cloud and radiation test bed site: 2. Effects of mixing height on aerosol properties, *J. Geophys. Res.*, 109, D06209, doi:10.1029/2003JD004024.

Draxler, R. R., and G. D. Rolph (2003), HYSPLIT (HYbrid Single-Particle Lagrangian Integrated Trajectory) Model, NOAA Air Resour. Lab., Silver Spring, Md. (Available at http://www.arl.noaa.gov/ready/hysplit4.html)

Gasparini, R., R. J. Li, and D. R. Collins (2004), Integration of size distributions and size-resolved hygroscopicity measured during the Houston Supersite for compositional categorization of the aerosol, *Atmos. Environ.*, 38(20), 3285–3303.

Gasparini, R., R. J. Li, D. R. Collins, and R. A. Ferrare (2006), Application of aerosol hygroscopicity measured at the ARM Southern Great Plains site to examine composition and evolution, *J. Geophys. Res.*, doi:10.1029/2004JD005448, in press.

Ghan, S. J., et al. (2006), Use of in situ cloud condensation nuclei, extinction, and aerosol size distribution measurements to test a method for retrieving cloud condensation nuclei profiles from surface measurements, *J. Geophys. Res.*, 111, D05S10, doi:10.1029/2004JD005752.

Intergovernmental Panel on Climate Change (2001), *Climate Change 2001: The Scientific Basis*, edited by J. T. Houghton et al., Cambridge Univ. Press, New York.

Iziomon, M. G., and U. Lohmann (2003), Characteristics and direct radiative effect of mid-latitude continental aerosols: The ARM case, *Atmos. Chem. Phys.*, 3, 1903–1917.

Jaffe, D., I. Bertschi, L. Jaegle, P. Novelli, J. S. Reid, H. Tanimoto, R. Vingarzan, and D. L. Westphal (2004), Long-range transport of Siberian biomass burning emissions and impact on surface ozone in western North America, *Geophys. Res. Lett.*, 31, L16106, doi:10.1029/2004GL020093.

Pahlow, M., G. Feingold, A. Jefferson, E. Andrews, J. A. Ogren, J. Wang, Y.-N. Lee, R. A. Ferrare, and D. D. Turner (2006), Comparison between lidar and nephelometer measurements of aerosol hygroscopicity at the Southern Great Plains Atmospheric Radiation Measurement site, *J. Geophys. Res.*, 111, D05S15, doi:10.1029/2004JD005646.

Patashnick, H., and G. Rupprecht (1986), Microweighing goes on-line in real time, *Ind. Res. Dev.*, 28(6), 74–78.

Pitzer, K. S. (1973), Thermodynamics of electrolytes. I. Theoretical basis and general equations, *J. Phys. Chem.*, 77(2), 268–277.

Pitzer, K. S., and G. Mayorga (1973), Thermodynamics of electrolytes. II. Activity and osmotic coefficients for strong electrolytes with one or both ions univalent, *J. Phys. Chem.*, 77(19), 2300–2308.

Pruppacher, H. R., and J. D. Klett (1997), *Microphysics of Clouds and Precipitation: Second Revised and Enlarged Edition With an Introduction to Cloud Chemistry and Cloud Electricity*, 954 pp., Springer, New York.

Radke, L. F., A. S. Hegg, P. V. Hobbs, and J. E. Penner (1995), Effects of aging on the smoke from a large forest fire, *Atmos. Res.*, 38(1–4), 315–332.

Roberts, G. C., and A. Nenes (2005), A continuous-flow streamwise thermal-gradient CCN chamber for atmospheric measurements, *Aerosol Sci. Technol.*, 39(3), 206–221.

Rogers, C., and P. Squires (1977), A new device for studies of cloud condensation nuclei active at low supersaturations, in *Ninth International Conference on Atmospheric Aerosols, Condensation, and Ice Nuclei*, edited by A. Roddy and T. O'Conner, pp. 96–100, Galway Univ., Galway, Ireland.

Rolph, G. D. (2003), Real-time Environmental Applications and Display sYstem (READY), NOAA Air Resour. Lab., Silver Spring, Md. (Available at http://www.arl.noaa.gov/ready/hysplit4.html)

Rood, M. J., D. S. Covert, and T. V. Larson (1987), Hygroscopic properties of atmospheric aerosols in Riverside, California, *Tellus, Ser. B*, 39, 383–397.

Schmid, B., et al. (2004), Measurement and modeling of vertically resolved aerosol optical properties and radiative fluxes over the ARM SGP site during the May 2003 Aerosol IOP, paper presented at Fourteenth ARM Science Team Meeting, U.S. Dep. of Energy, Albuquerque, N. M.

Sheridan, P. J., D. J. Delene, and J. A. Ogren (2001), Four years of continuous surface aerosol measurements from the Department of Energy's Atmospheric Radiation Measurement Program Southern Great Plains Cloud and Radiation Testbed site, *J. Geophys. Res.*, 106(D18), 20,735–20,747.

Stolzenburg, M., N. Kreisberg, and S. Hering (1998), Atmospheric size distributions measured by differential mobility particle size spectrometry, *Aerosol Sci. Technol.*, 29(5), 402–418.

Tang, I. N., and H. R. Munkelwitz (1994), Water activities, densities, and refractive indices of aqueous sulfates and sodium nitrate droplets of atmospheric importance, *J. Geophys. Res.*, 99(D9), 18,801–18,808.

Twomey, S. (1977), *Atmospheric Aerosols*, 302 pp., Elsevier, New York.

VanReken, T. M., T. A. Rissman, G. C. Roberts, V. Varutbangkul, H. H. Jonsson, R. C. Flagan, and J. H. Seinfeld (2003), Toward aerosol/cloud condensation nuclei (CCN) closure during CRYSTAL-FACE, *J. Geophys. Res.*, 108(D20), 4633, doi:10.1029/2003JD003582.

Wang, J., et al. (2002), Clear-column radiative closure during ACE-Asia: Comparison of multiwavelength extinction derived from particle size and composition with results from Sun photometry, *J. Geophys. Res.*, 107(D23), 4688, doi:10.1029/2002JD002465.

Wang, J., R. C. Flagan, and J. H. Seinfeld (2003), A Differential Mobility Analyzer (DMA) system for submicron aerosol measurements at ambient relative humidity, *Aerosol Sci. Technol.*, 37(1), 46–52.

Wang, S. C., and R. C. Flagan (1990), Scanning electrical mobility spectrometer, *Aerosol Sci. Technol.*, 13(2), 230–240.

Weber, R. J., D. Orsini, Y. Daun, Y.-N. Lee, P. J. Klotz, and F. Brechtel (2001), A particle-into-liquid collector for rapid measurement of aerosol bulk composition, *Aerosol Sci. Technol.*, 35(3), 718–727.

————————————

F. J. Brechtel, Brechtel Manufacturing, Inc., Hayward, CA 94544, USA.

D. R. Collins and R. Gasparini, Department of Atmospheric Sciences, Texas A&M University, College Station, TX 77843-3150, USA.

R. C. Flagan, T. A. Rissman, J. H. Seinfeld, and T. M. VanReken, Department of Chemical Engineering, California Institute of Technology, Pasadena, CA 91125, USA. (seinfeld@caltech.edu)

H. H. Jonsson, Center for Interdisciplinary Remotely Piloted Aircraft Studies, United States Naval Postgraduate School, Marina, CA 93933, USA.

J. Wang, Brookhaven National Laboratory, Upton, NY 11973, USA.